



**HAL**  
open science

## NMR-based isotopic and isotopomic analysis

Serge Akoka, Gérald S. Remaud

► **To cite this version:**

Serge Akoka, Gérald S. Remaud. NMR-based isotopic and isotopomic analysis. Progress in Nuclear Magnetic Resonance Spectroscopy, 2020, 120-121, pp.1-24. 10.1016/j.pnmrs.2020.07.001 . hal-03374968

**HAL Id: hal-03374968**

**<https://nantes-universite.hal.science/hal-03374968>**

Submitted on 22 Aug 2022

**HAL** is a multi-disciplinary open access archive for the deposit and dissemination of scientific research documents, whether they are published or not. The documents may come from teaching and research institutions in France or abroad, or from public or private research centers.

L'archive ouverte pluridisciplinaire **HAL**, est destinée au dépôt et à la diffusion de documents scientifiques de niveau recherche, publiés ou non, émanant des établissements d'enseignement et de recherche français ou étrangers, des laboratoires publics ou privés.



Distributed under a Creative Commons Attribution - NonCommercial 4.0 International License

## NMR-based isotopic and isotopomic analysis

Serge Akoka\*, Gérald S. Remaud

Université de Nantes, CNRS, CEISAM UMR 6230, F-44000 Nantes, France

**\*Corresponding author:** Serge AKOKA

Chimie et Interdisciplinarité: Synthèse, Analyse, Modélisation (CEISAM), UMR 6230, Faculté des Sciences, BP 92208, 2 rue de la Houssinière, F-44322 Nantes Cedex 03, France.

Tel. +33(0)2 51 12 57 07 ; E-mail: [serge.akoka@univ-nantes.fr](mailto:serge.akoka@univ-nantes.fr)

Gérald Remaud, Chimie et Interdisciplinarité: Synthèse, Analyse, Modélisation (CEISAM), UMR 6230, Faculté des Sciences, BP 92208, 2 rue de la Houssinière, F-44322 Nantes Cedex 03, France.

Tel. +33(0)2 51 12 57 19 ; E-mail: [gerald.remaud@univ-nantes.fr](mailto:gerald.remaud@univ-nantes.fr)

72 Pages

25 figures

3 tables

**Key words:** Isotopic analysis, irm-NMR, Quantitative NMR, High accuracy, PSIA

## 1 **Abstract**

2 Molecules exist in different isotopic compositions and most of the processes, physical or chemical, in  
3 living systems cause selection between heavy and light isotopes. Thus, knowing the isotopic  
4 fractionation of the common atoms, such as H, C, N, O or S, at each step during a metabolic pathway  
5 allows the construction of a unique isotope profile that reflects its past history. Having access to the  
6 isotope abundance gives valuable clues about the (bio)chemical origin of biological or synthetic  
7 molecules. Whereas the isotope ratio measured by mass spectrometry provides a global isotope  
8 composition, quantitative NMR measures isotope ratios at individual positions within a molecule. We  
9 present here the requirements and the corresponding experimental strategies to use quantitative  
10 NMR for measuring intramolecular isotope profiles. After an introduction showing the historical  
11 evolution of NMR for measuring isotope ratios, the vocabulary and symbols - for describing the  
12 isotope content and quantifying its change - are defined. Then, the theoretical framework of very  
13 accurate quantitative NMR is presented as the principle of Isotope Ratio Measurement by NMR  
14 spectroscopy, including the practical aspects with nuclei other than  $^2\text{H}$ , that have been developed  
15 and employed to date. Lastly, the most relevant applications covering three issues, tackling  
16 counterfeiting, authentication, and forensic investigation, are presented, before giving some  
17 perspectives combining technical improvements and methodological approaches.

18

19	<b>Table of contents</b>	
20	<b>1. Introduction .....</b>	<b>5</b>
21	<b>2. Isotopic analysis.....</b>	<b>10</b>
22	2.1. Isotopologues, isotopomers and isotopic quantities .....	10
23	2.2. Isotope fractionation.....	11
24	2.3. Interest of NMR for isotope analysis.....	13
25	<b>3. High accuracy quantitative NMR.....</b>	<b>17</b>
26	3.1. Trueness, precision and accuracy.....	17
27	3.2. Is NMR always quantitative?.....	17
28	3.3. Parameters influencing trueness.....	18
29	3.4. Parameters influencing precision.....	23
30	3.5. Experimental conditions for high accuracy quantitative NMR.....	27
31	<b>4. Isotope ratio measurement by NMR.....</b>	<b>30</b>
32	4.1. Isotopic fingerprinting .....	30
33	4.2. Position-specific isotope abundance measurement .....	30
34	4.3. Practical aspects .....	35
35	<b>5. Applications.....</b>	<b>38</b>
36	5.1. Sample preparation.....	38
37	5.2. Counterfeiting .....	40
38	5.3. Forensic investigations .....	44
39	5.4. Authentication.....	50
40	5.5. Multi-omics approach .....	56
41	<b>6. Concluding remarks and perspectives.....</b>	<b>59</b>
42	<b>Acknowledgements .....</b>	<b>61</b>
43	<b>References .....</b>	<b>62</b>
44	<b>Glossary of abbreviations.....</b>	<b>69</b>

45	Acronyms and notations for NMR.....	69
46	Isotope terms .....	70
47	Other notations.....	71
48		
49		

## 50 1. Introduction

51 Molecules exist in different isotopic compositions in which the heavy element distributions depend  
52 on the processes and raw materials used for making the component. Most of the processes, physical  
53 or chemical, in living systems cause selection between heavy and light isotopes. Thus, knowing the  
54 isotopic fractionation of the common atoms, such as H, C, N, O or S, at each step during a synthetic  
55 or metabolic process leads to the construction of a unique isotope profile that reflects the past  
56 history of the molecule. Having access to the isotopic abundances gives valuable clues about the  
57 (bio)chemical origins of molecules [1].

58 There are several techniques for determining isotope ratios [2 and refs. within]. Mass spectrometry  
59 (irm-MS: isotope ratio measurement by Mass Spectrometry, also known as IRMS: Isotope Ratio by  
60 Mass Spectrometry) was used first. Irm-MS is designed to measure the isotope abundance in  
61 targeted gases introduced into the source of the spectrometer. For example, CO<sub>2</sub> and N<sub>2</sub> are the  
62 gases used to determine <sup>13</sup>C/<sup>12</sup>C and <sup>15</sup>N/<sup>14</sup>N ratios. Organic matter is converted into these gases via  
63 the successive oxidation and reduction furnaces of an elemental analyzer. Then, the ratios  
64 <sup>13</sup>CO<sub>2</sub>/<sup>12</sup>CO<sub>2</sub> or <sup>15</sup>N<sub>2</sub>/<sup>14</sup>N<sub>2</sub> are measured after appropriate calibrations, and the result is expressed as  
65 the global (or bulk) isotopic composition: δ<sup>13</sup>C<sub>g</sub> and δ<sup>15</sup>N<sub>g</sub> (see Section 2 for definitions of symbols).  
66 Irm-MS has two main advantages: instrumental automation, and the requirement for only a small  
67 amount of material (routinely a few mg) [3]. Later, hyphenated methodologies were developed, such  
68 as chromatographic coupling: liquid chromatography (LC-irm-MS) and, mainly, gas chromatography  
69 (GC-irm-MS), leading to so-called CSIA (Compound Specific Isotope Analysis) [4].

70 However, only the average contribution of all the <sup>13</sup>C or <sup>15</sup>N isotopomers and isotopologues (these  
71 and other relevant terms are explained in section 2) present in the compound is determined leading  
72 to one overall parameter, δ<sup>13</sup>C<sub>g</sub> or δ<sup>15</sup>N<sub>g</sub>. The intramolecular isotope distribution is thus not  
73 accessible, unless indirect measurements are made on fragments. The oldest approach to position-  
74 specific isotope analysis (PSIA) is the chemical and/or enzymatic degradation of the molecule, with

75 subsequent analysis of the resulting fragments by irm-MS. A less tedious methodology was  
76 developed through on-line pyrolysis and GC separation of fragments coupled with mass  
77 spectrometry [5]. However, this is currently restricted to small molecules such as acetic acid, lactic  
78 acid or ethanol [6].

79 Whereas the isotope ratio measured by Mass Spectrometry (irm-MS) provides a global isotope  
80 composition, *e.g.*  $\delta^{13}\text{C}_g$ , quantitative NMR measures isotope ratios at individual positions (sites) of a  
81 molecule (irm-NMR: isotope ratio measured by NMR, also known as SNIF-NMR<sup>TM</sup>: Site-Specific  
82 Natural Isotope Fractionation determined by NMR). By separating and quantitating each isotopomer,  
83 irm-NMR resolves isotope fractionation at natural abundance for every position in target molecules.  
84 Historically, the use of NMR spectroscopy for isotope ratio measurement was pioneered by Martin  
85 and Martin in the early 1980s, applying quantitative  $^2\text{H}$  NMR to ethanol for the detection of over-  
86 chaptalized wines [7]. Despite its very low sensitivity, deuterium has some favorable characteristics  
87 for quantitative NMR: (i) the predominance of quadrupolar relaxation avoids perturbations in signal  
88 intensities due to the nOe (nuclear Overhauser effect), (ii) longitudinal relaxation times ( $T_1$ ) are not  
89 too long and (iii) the large array of isotope effects (isotopic composition range around 500‰) means  
90 that the precision needed for irm- $^2\text{H}$  NMR is only of the order of a few percent. As a result, various  
91 applications have been published over the last 30 years in areas covering the authenticity of flavors  
92 and food, counterfeiting of medicines, and forensic investigations [8]. In 1988, irm- $^2\text{H}$  NMR was  
93 adopted by the International Office of Vines and Wine (OIV) and by the EEC and became the official  
94 method to detect sugar addition in wine, and to determine the origins of vanillin and acetic acid [8].  
95 A remarkable development of irm- $^2\text{H}$  NMR was achieved in chirally oriented media, which makes  
96 accessible residual anisotropic intramolecular NMR interactions while preserving high spectral  
97 resolution. In such an environment, enantiomers of chiral molecules or enantiopic elements of  
98 prochiral produce distinct NMR signals, giving access to unique information. That led to a  
99 fundamental understanding of the enzymatic processes (stereoselectivity) of natural  $^2\text{H}$  distribution  
100 in prochiral molecules [9].

101 Nevertheless, there are some limitations of irm-<sup>2</sup>H NMR that are not (or are only partly)  
102 compensated by using a very high magnetic field and cryoprobe. The amount of material needed for  
103 analysis is relatively high, *e.g.* 1 g for irm-<sup>2</sup>H NMR on vanillin in routine analysis on a 400/500 MHz  
104 spectrometer, prohibiting the study of minute amounts of compound. Furthermore, the hydrogen  
105 atom (and therefore <sup>2</sup>H) is often easily exchangeable. These and other problems of irm-<sup>2</sup>H NMR have  
106 been circumvented by studying nuclei such as <sup>13</sup>C or <sup>15</sup>N. However, the performance that must be  
107 reached to determine isotope ratios is 10 times higher for <sup>13</sup>C (or for <sup>15</sup>N) than for <sup>2</sup>H, since the range  
108 of variability of <sup>13</sup>C isotopic compositions is restricted to 50‰ in natural products, leading to a  
109 required precision better than 1‰ (or 0.1%) [10]. For comparison, the precision of irm-MS is 0.3‰ in  
110 routine analysis for the determination of δ<sup>13</sup>C<sub>g</sub> on organic matter. During the same period as <sup>2</sup>H NMR  
111 was being developed, several attempts were made to establish a methodology for irm-<sup>13</sup>C NMR with  
112 reproducible data, but these achieved only moderate results [11, 12]. However, 15 years ago the  
113 major source of irreproducibility was identified as the efficiency of the <sup>1</sup>H decoupling, because of its  
114 variation over the range of proton frequencies. Once this obstacle had been overcome, reproducible  
115 results were obtained [13, 14] on reduced amounts of sample, providing valuable further information  
116 compared to <sup>2</sup>H NMR. The method was named irm-<sup>13</sup>C NMR 'single-pulse' (<sup>13</sup>C excitation followed by  
117 inverse gated decoupling, as opposed to the multi-pulse methodology). For example, the analysis of  
118 vanillin can be performed on 250 mg, instead of 1 g for irm-<sup>2</sup>H NMR, with even more discriminating  
119 parameters [15]. The application of this single-pulse approach provided a range of results not  
120 previously accessible, including the counterfeiting of active pharmaceutical ingredients (APIs), the  
121 metabolism of photosynthesis and post-photosynthesis, the authenticity of natural products, and  
122 sorption and evaporation phenomena.

123 The most outstanding finding from these data was the occurrence of normal (<sup>12</sup>C is favored) and  
124 inverse (<sup>13</sup>C is favored) isotope effects during the same process. In addition, long-range isotope  
125 effects were also observed. Advanced modeling of isotope fractionation and mechanisms of  
126 transformation confirmed that the intramolecular isotope distribution provides many more details,



127 which could be missed when using the global value from irm-MS. A strong argument can then be put  
128 forward to answer the question: if there is no change in  $\delta^{13}\text{C}_g$  during a transformation (between  
129 substrate and product), does this mean that there is no fractionation within the molecule? The  
130 answer given by PSIA is usually no, because there is a counteractive contribution of normal and  
131 inverse intramolecular isotope effects at different positions, generating an average close to zero.

132 Despite these important contributions, the single-pulse method has some limitations, because the  
133 amount of pure molecule required remains too high and the analysis duration too long for many  
134 applications. Clearly, an increase in molecular weight will make irm- $^{13}\text{C}$  NMR 'single-pulse' difficult. In  
135 contrast to  $^2\text{H}$ , because  $^{13}\text{C}$  has a spin of  $\frac{1}{2}$ , it is easy to use multi-pulse sequences for sensitivity  
136 and/or resolution improvement. The challenge inherent in achieving the high precision (about 1‰)  
137 required for isotopic measurement is: what are the modifications that should be made to a pulse  
138 sequence to achieve exact and robust data? This is particularly important for refocusing and  
139 inversion with  $\pi$  pulses. A thorough investigation of the polarization transfer sequences, namely  
140 DEPT and INEPT, showed that adiabatic pulses provide robust and very reproducible  $^{13}\text{C}$  profiles in a  
141 short time or with less product. With shorter repetition time (TR) and polarization transfer, a gain in  
142 sensitivity of six- to ten-fold can be obtained depending on the studied molecule [16].

143 However, with such sequences, quaternary carbons are not observed, and the intensity of a signal  
144 depends on the values of the delays used in the polarization transfer. This is to say that the area of  
145 the signal is not solely proportional to the number of nuclei giving this signal, but also depends on  
146 pulse sequence parameters. Nevertheless, this apparent isotope composition (see Section 4.2 for  
147 further details) will change from one sample to another due to the change in the  $^{13}\text{C}$  amount. The  
148 resulting profiles can be used as input data for omics interpretation: the concept of isotopomics at  
149 natural abundance was then introduced (this term was first used for mapping the isotopic  
150 distribution over metabolites upon  $^{13}\text{C}$  labeling [17]). In some cases, the number of quaternary  
151 carbons is not negligible and information is undoubtedly lost. The delay for the transfer of  
152 polarization in INEPT can be adjusted to long-range  $^1\text{H}$ - $^{13}\text{C}$  couplings ( $^n\text{J}_{13\text{C}-1\text{H}}$ ). The resulting

153 methodology was named Full-Spectrum INEPT (FS-INEPT) [18]. It was tested for  $^{13}\text{C}$  profiling (showing  
154 that full  $^{13}\text{C}$  profiles could be obtained for 40 mg of caffeine or acetaminophen in a short time) as  
155 well as for  $^{15}\text{N}$  [19] for which it is the only way to observe isotope effects.

156 The present article aims to present the requirements and the corresponding experimental strategies  
157 for using quantitative NMR to measure intramolecular isotope profiles. Several questions are  
158 addressed in order to help the reader identify both the potential and the constraints of isotope ratio  
159 measurement by NMR spectroscopy (irm-NMR). (i) What are the areas of interest for isotope  
160 composition? (ii) How is the isotope content expressed? (iii) What is measured according to the  
161 technique used? (iv) What are the conditions for quantitative NMR to reach appropriate accuracy?  
162 (v) Are there typical examples of applications of irm-NMR?

163 In this review, the answers to these questions are organized as follows: after this Introduction  
164 describing the historical evolution of NMR for measuring isotope ratios, we define in Section 2 the  
165 vocabulary and symbols used for describing the isotope content and for quantifying its change.  
166 Section 3 covers the theoretical framework of quantitative NMR within the constraint of a very high  
167 accuracy level, defined as trueness and precision. In Section 4, we detail the principle of isotope ratio  
168 measured by NMR spectroscopy (irm-NMR), including practical aspects with nuclei other than  $^2\text{H}$ ,  
169 that have been developed and employed to date. In Section 5, we present and discuss the most  
170 relevant applications covering three issues: tackling counterfeiting, authentication and forensic  
171 investigation. In that Section, we also stress the rules for preparing samples without isotope  
172 fractionation. Finally, we conclude with some perspectives combining technical improvements and  
173 methodological approaches.

174

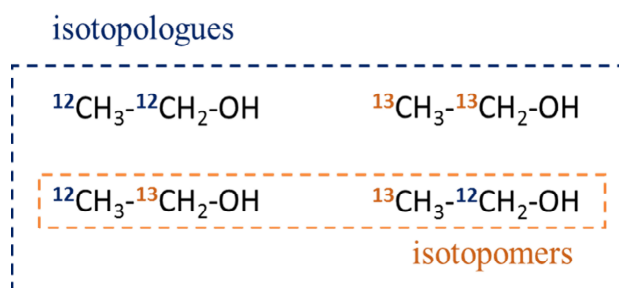
## 175 2. Isotopic analysis

### 176 2.1. Isotopologues, isotopomers and isotopic quantities

177 As mentioned in the Introduction, heavy isotopes, such as  $^2\text{H}$  or  $^{13}\text{C}$ , are not uniformly distributed in a  
178 molecule; this leads to different isomers which are called isotopologues. When two isotopologues  
179 have the same number of positions occupied by a given isotope, they are called isotopomers (**Fig. 1**).

180 In the case of light elements (H, C, N, O), the average abundances of heavy isotopes are small and so  
181 the probability of finding two heavy isotopes in the same isotopologue is very low. Consequently,  
182 most isotopologues detected by NMR at natural abundance are mono-labeled isotopomers.

183



184

185 **Fig. 1:** Difference between isotopologues and isotopomers, illustrated for carbon atoms in ethanol.

186 Isotopologues differ only in their isotope compositions, whereas isotopomers have the same numbers of  
187 isotopes but in different positions. Reprinted with permission from Ref. [21]. Copyright 2017 Magnetic

188 Resonance in Chemistry.

189

190

191 In order to quantify the isotope distribution between different molecules or within a given molecule,  
192 different expressions are routinely used (**Table 1**). For the element  $E$ , the isotope ratio ( $R$ ) measures  
193 the relative amount of the heavier isotope ( $^hE$ ) compared to the lighter one ( $^lE$ ), while the isotope  
194 abundance ( $x$ ) measures the relative amount of the heavier isotope ( $^hE$ ) compared to the total  
195 amount of element  $E$  [20]. It should be noted that for hydrogen and oxygen, the isotope ratio and

196 isotope abundance have almost the same value because of the very small amount of heavy isotopes,  
197 but this is not the case for all elements, notably carbon.

198 For carbon and nitrogen, the range and variation of values observed are very small (a few percent),  
199 therefore it is preferable to use isotope composition ( $\delta$ ). This expresses the relative value (in permil,  
200 ‰) of the isotope ratio against an international standard (**Table 1**) [21].

201

202 **Table 1:** Relations defining the main expressions used in isotope analysis for an element  $E$  with two isotopes.

203 The heavier and lighter isotopes are noted  $^hE$  and  $^lE$ , respectively. *Std* indicates the international standard used

204 to express the  $\delta$  value.

---

Isotope ratio ( $R$ )	Isotope abundance ( $x$ )	Isotope composition ( $\delta$ )
$R(^hE/^lE) = \frac{N(^hE)}{N(^lE)}$	$x(^hE/^lE) = \frac{N(^hE)}{N(^hE) + N(^lE)}$	$\delta^hE_{std} = \left( \frac{R(^hE/^lE)}{R(^hE/^lE)_{std}} - 1 \right) \cdot 1000$

---

205

206 For the NMR community, this  $\delta$  should not be confused with the use of  $\delta$  for chemical shifts. The  
207 standard compounds employed are Vienna Pee Dee Belemnite and atmospheric  $N_2$  (standard  
208 calibrated by IAEA (Vienna)) for  $^{13}C$  and  $^{15}N$ , respectively, although these are now routinely used via a  
209 calibrated intermediate compound.

## 210 **2.2. Isotope fractionation**

211 The fractionation between heavy and light isotopes is the result of the kinetic and thermodynamic  
212 isotope effects that lead to the selection of one isotope in preference to the other. As described in  
213 Section 2.1, isotopologues can differ in: (i) the type of elements and the corresponding isotopes;  
214 and/or (ii) the isotope itself; and/or (iii) the number of atoms of isotope; and/or (iv) the isotope  
215 positions within the molecule. All these molecules can behave differently according to the process  
216 involved: different masses result in different bond frequencies that lead to different zero-point

217 energies and therefore to changes in rates and in equilibria. Without going deeply into the  
218 theoretical aspects, it will suffice here to describe the essentials needed to understand what is  
219 measured and for what purpose [23]. The vibrational zero-point energy is lower for a bond involving  
220 a heavier isotope of an element, *i.e.* such bonds will be stronger. The energy of the system is  
221 minimized when the heavy isotope is at the position with the strongest bond. This is what is  
222 observed at equilibrium. Thus, we can distinguish the kinetic isotope effect (KIE) from the equilibrium  
223 isotope effect (EIE). In general, there are other contributions to the kinetic effect during a chemical  
224 reaction (steric, vibrational modes) usually leading to the normal isotope effect, in which the light  
225 species is favored, or the inverse isotope effect, in which the heavy species is favored (in this case,  
226 there is probably a contribution from a process at equilibrium). Depending on the scientific field, the  
227 isotope fractionation is expressed in different ways. The isotope effect is named  $\alpha$ . During a  
228 transformation between A and B,  $\alpha$  is given by Eq. (1):

$$229 \quad \alpha_{A-B} = \frac{R_A}{R_B} \quad (1)$$

230 For a kinetic isotope effect,  $R_A$  is the isotope ratio of the substrate A and  $R_B$  that of the product  
231 obtained during a first-order reaction from A. For a thermodynamic effect (equilibrium), A is in  
232 equilibrium with B and the isotope ratios R are those at equilibrium. In biology, the fractionation is  
233 expressed as  $\Delta = \alpha - 1$ , where  $\alpha > 1$  corresponds to a normal effect ( $\Delta > 0$ ) and  $\alpha < 1$  to an inverse  
234 effect ( $\Delta < 0$ ). In geoscience, the fractionation is related to the enrichment factor  $\varepsilon$  by Eq. (2):

$$235 \quad \varepsilon = (\alpha - 1) \times 1000 \quad (2)$$

236 However, in this case,  $\alpha$  is the reverse of the previous one used in biological studies, and  $\varepsilon$  should be  
237 considered as  $\varepsilon = -\Delta$ . This will also invert the definition of the sense of fractionation. Readers of the  
238 publications cited in this review should be aware of the particular convention used for the work  
239 being described, by checking what rules are used by the authors to define a 'normal' or an 'inverse'  
240 isotope effect.

241 We present herein only one type of fractionation, that is relevant for interpreting applications  
242 related to plant origins: the photosynthetic pathways, *i.e.* the change in  $\delta^{13}\text{C}$  according to the  
243 mechanism involved during the assimilation of atmospheric  $\text{CO}_2$  during photosynthesis [10]. There  
244 are three metabolic processes, known as  $\text{C}_3$ ,  $\text{C}_4$  and CAM. This notation is associated with the number  
245 of carbon atoms of the molecule first synthesized upon carboxylation: for  $\text{C}_3$  it is 3-phosphoglycerate  
246 (direct Calvin cycle); for  $\text{C}_4$  it is oxaloacetate (intermediate prior to the Calvin cycle). The third  
247 strategy, CAM (Crassulacean Acid Metabolism), is an adaptation of the plant to water stress and is  
248 similar to  $\text{C}_4$  but with different activity during night and day, associated with stomatal conductance: a  
249 contribution to the direct Calvin cycle is then possible, but via the  $\text{C}_4$  mechanism. A very  
250 characteristic  $^{13}\text{C}$  fractionation relative to the  $\delta^{13}\text{C}$  of atmospheric  $\text{CO}_2$  is found [24] for each  
251 photosynthetic pathway, that is constant over the earth, *i.e.*  $\approx -8\text{‰}$ . A global fractionation of the  
252 order of  $-20\text{‰}$  and  $-4\text{‰}$  is observed for  $\text{C}_3$  and  $\text{C}_4$  plants, respectively, *e.g.*  $\delta^{13}\text{C}_g \approx -26$  to  $-29\text{‰}$  and  $\approx -$   
253  $10$  to  $-12\text{‰}$  for sucrose in beet ( $\text{C}_3$ ) and in sugar cane ( $\text{C}_4$ ), respectively. For CAM plants, the  
254 fractionation depends on the plant and may be around  $-20\text{‰}$ , as for vanilla ( $\delta^{13}\text{C}_g$  of vanillin ex-bean  
255 =  $-20\text{‰}$ ), or close to the  $\text{C}_4$  plant value, as for pineapple ( $\delta^{13}\text{C}_g \approx -12\text{‰}$  of sugars in pineapple juice).

### 256 **2.3. Interest of NMR for isotope analysis**

257 In routine isotope analysis, global isotope abundance ( $x_g$ ) is determined, most often using irm-MS  
258 [25, 26]. The main problem here is that isotope fractionation induces an intramolecular difference in  
259 the isotope amount, which can only be observed if the contribution at each position can be  
260 distinguished. In fact, the effect on the isotope ratio from a given position is diluted by the isotope  
261 ratios at all the other positions of the compound. It can thus fall below the detection threshold as  
262 soon as the molecule contains more than five or six carbons [27].

263 Several methods have been proposed to measure position-specific isotope compositions. The earliest  
264 involved chemically cleaving the analyte then analyzing the fragments separately by irm-MS [28].  
265 More recently, GC-irm-MS was modified to perform position-specific isotope analysis (PSIA) [29] but

266 to date this technique is limited to molecules with a small number of carbons. High resolution mass  
267 spectrometry has also been adapted to measure clumped and position-specific isotope compositions  
268 [30]. It works on a very small sample but, like the previous method, MS-based isotope analysis is  
269 limited to small organic molecules. Furthermore, isotope fractionations that occur during analysis  
270 have not been successfully addressed. Therefore, the accuracy of this method has not yet been  
271 assessed by other proven methods.

272 On the other hand, NMR is an excellent method to perform PSIA since each isotope can be measured  
273 separately using its own resonance frequency, and each molecular position can be distinguished by  
274 its chemical shift (**Fig. 2**). Moreover, peak areas are directly proportional to the number of detected  
275 nuclei, and therefore to the isotope abundance ( $x_i$ ) of the considered position  $i$ . The signal detected  
276 for position  $i$  is given by Eq. (3):

$$277 \quad S_i = k \cdot n_i \cdot c \cdot x_i \quad (3)$$

278 where  $n_i$  is the number of equivalent nuclei at position  $i$  and  $c$  the concentration of the measured  
279 compound.

280 The molar fraction of each isotopomer can then be calculated using Eq. (4) [31]:

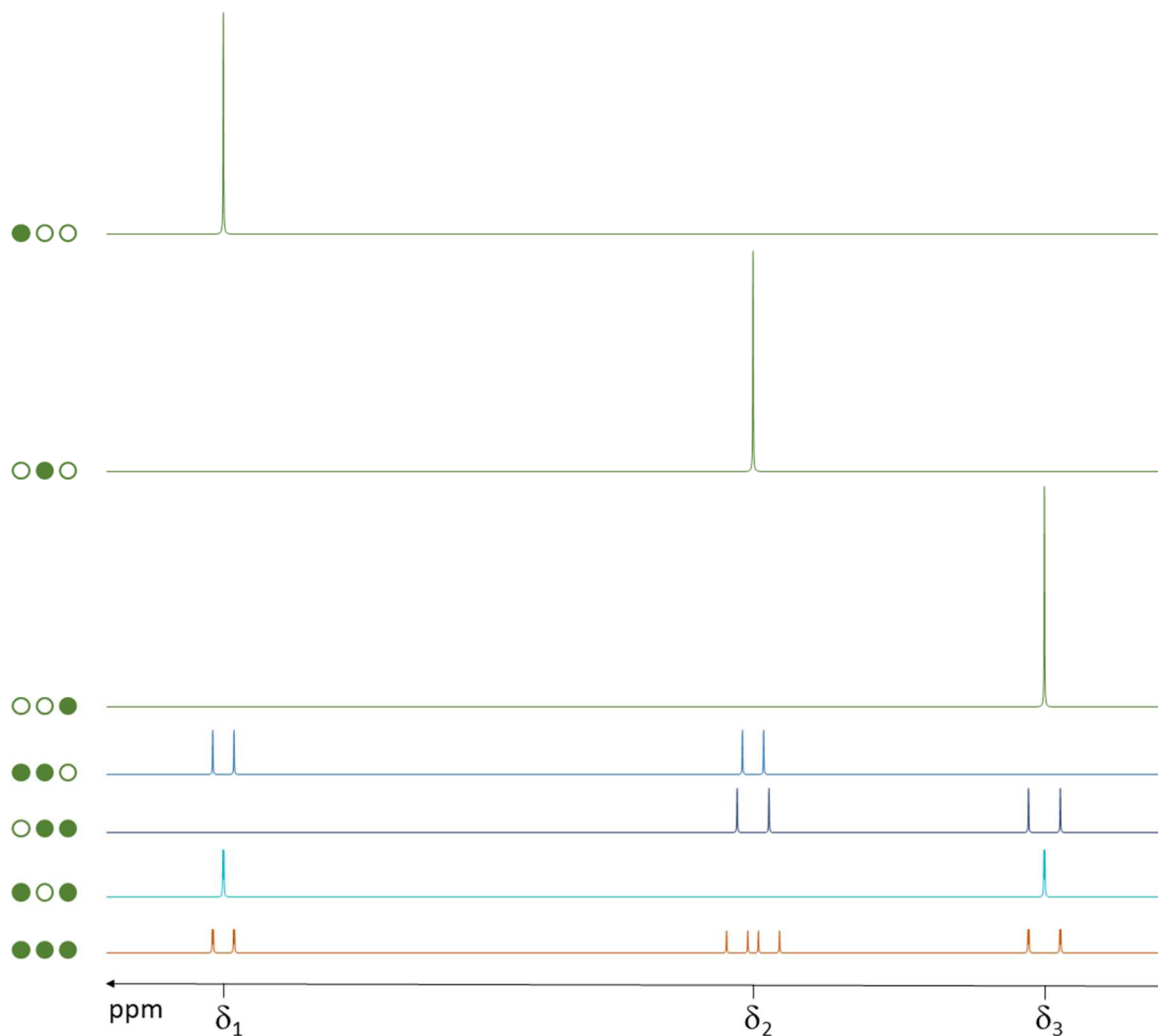
$$281 \quad f_i = \frac{S_i}{\sum S_i} \quad (4)$$

282 The set of  $f_i$  provides an isotopic profile directly, which can be used to trace or authenticate a  
283 compound [21, 22, 31]. It can also be used to obtain the specific abundances using two methods [31].  
284 Either a reference compound of known isotope abundance is added to the sample, or the global  
285 isotope abundance  $x_g$  is obtained by a method other than NMR. These two approaches are  
286 developed in Section 4.

287 However, this is only possible if the measurement accuracy is better than the variations observed in  
288 isotope abundance at natural abundances. The performance to be reached for the determination of  
289 isotope ratios is 10 times higher for  $^{13}\text{C}$  (or for  $^{15}\text{N}$ ) than for  $^2\text{H}$ , since the range of variability of the

290 isotopic  $^{13}\text{C}$  compositions is restricted to 50‰ in natural products, leading to a required precision  
291 better than 1‰ (or 0.1%). For comparison, the precision of irm-MS is 0.3‰ in routine analysis for the  
292 determination of  $\delta^{13}\text{C}_g$  [21, 22, 31].

293



294

295 **Fig. 2:**  $^{13}\text{C}$ -NMR signals from a three-carbon molecule. Filled circles indicate positions occupied by a  $^{13}\text{C}$  and  
296 open circles indicate positions occupied by a  $^{12}\text{C}$ . The contributions of bi-labelled isotopologues are equivalent  
297 and are assumed to be close to the average abundance 1.1% each, since NMR will not be able to distinguish  
298 small variations around this average value. Signal from the tri-labelled isotopologue theoretically contributes  
299 but its abundance is too low to be detected by NMR with current techniques. The observed spectrum  
300 consists in the addition of all these contributions.



301 This explains why  $^2\text{H}$  was the first nucleus used for irm-NMR. However, as previously mentioned, irm-  
 302  $^2\text{H}$  NMR has some limitations in terms of low sensitivity, restricted chemical shift range leading to  
 303 signal overlap, and small dynamic range; a molecular weight above  $250 \text{ g}\cdot\text{mol}^{-1}$  results in  $^2\text{H}$  NMR  
 304 spectra with low resolution due to efficient relaxation. These are not (or are only partly)  
 305 compensated by using a very high magnetic field and cryoprobe, prohibiting the study of compounds  
 306 found in final matrices or in environmental samples. Furthermore, the hydrogen atom (and therefore  
 307  $^2\text{H}$ ) is in many cases easily exchangeable. All these problems are circumvented by studying a nucleus  
 308 such as  $^{13}\text{C}$  (or even  $^{15}\text{N}$ ). The intrinsic NMR properties of  $^{13}\text{C}$  are clearly much more favorable than  
 309 those of  $^2\text{H}$ , as summarized in **Table 2**.

310 However, the requirement for nOe suppression, combined with the long  $^{13}\text{C}$   $T_1$  values, and the high  
 311 signal-to-noise ratio (SNR), leads to long measurement times. Nevertheless, by using a relaxation  
 312 reagent (such as tris(2,4-pentadionato)chromium(III) [CrAcac]) PSIA by irm- $^{13}\text{C}$  NMR can be  
 313 performed in a reasonable time-frame [14].

314

315 **Table 2:** Main properties of nuclei used in irm-NMR

	$^2\text{H}$	$^{13}\text{C}$	$^{15}\text{N}$	$^{17}\text{O}$
Magnetogyric ratio ( $10^6 \text{ rad}\cdot\text{s}^{-1}\cdot\text{T}^{-1}$ )	41.066	67.262	-27.116	-36.279
Mean abundance (%)	0.02	1.08	0.37	0.04
Sensitivity / $^1\text{H}$	$1.4 \cdot 10^{-6}$	$1.8 \cdot 10^{-4}$	$3.8 \cdot 10^{-6}$	$1.1 \cdot 10^{-5}$
Spin	1	1/2	1/2	5/2

316

317

### 318 **3. High accuracy quantitative NMR**

319 In this Section, we describe the conditions needed to reach the high accuracy required for isotopic  
320 NMR, after first defining the notions of trueness, precision and accuracy, since these words can take  
321 different meanings in different disciplines.

#### 322 **3.1. Trueness, precision and accuracy**

323 In the field of isotope ratio measurement by NMR (irm-NMR), the definitions used for these three  
324 quantities are those proposed by Menditto *et al.* [32] and incorporated by the VIM (International  
325 Vocabulary of Metrology) in its third edition [33]. The reader will find a further critical overview in  
326 [34]. Precision is “the closeness of agreement between independent test results obtained under  
327 stipulated conditions”, and therefore characterizes random errors. Trueness is “the closeness of  
328 agreement between the average value obtained from a large series of test results and an accepted  
329 reference value”, and therefore characterizes systematic errors. Accuracy is the combined  
330 contribution of both precision and trueness.

#### 331 **3.2. Is NMR always quantitative?**

332 In the NMR literature, the notion of quantitative NMR (qNMR) most often implies that the  $k$   
333 coefficient of Eq. (3) is identical for all the positions  $i$ . However, this definition of qNMR is much too  
334 restrictive, notably because it excludes 1D and nD acquisitions performed with multi-pulse  
335 sequences. If such a constraint was applied to other analytical techniques, such as optical  
336 spectroscopies, chromatography or mass spectrometry, no quantitative measurement would be  
337 possible.

338 In fact, when the precision is good enough (with respect to the given objective), trueness can be  
339 reached by a calibration procedure, such as external calibration curves, or with an internal added  
340 standard [35]. Consequently, as described below, all NMR sequences can be used for quantitative  
341 analysis if they have been previously optimized in order to obtain the target repeatability.

### 342 **3.3. Parameters influencing trueness**

#### 343 **3.3.1. Partial saturation**

344 Because of the signal-to-noise ratio (SNR) or phase cycling, multiple FIDs are usually accumulated  
345 before Fourier transform. For this purpose, the pulse sequence is repeated and a steady state is  
346 gradually established during the early scans [36]. In the case where each scan is preceded by a single  
347 RF observe pulse, the longitudinal magnetization present before the pulse reaches the equilibrium  
348 value:

$$349 \quad M_{eq} = M_0 \cdot \frac{(1 - \cos(\beta)) \cdot e^{-\frac{TR}{T_1}}}{1 - \cos(\beta) \cdot e^{-\frac{TR}{T_1}}} \quad (5)$$

350 where  $\beta$  is the flip angle induced by the RF pulse,  $TR$  is the repetition time and  $T_1$  is the longitudinal  
351 relaxation time [36].

352 The maximal amplitude for the detected signal is then obtained when  $\beta$  is equal to the so-called  
353 Ernst angle ( $\beta_E = \arccos(e^{-\frac{TR}{T_1}})$ ) calculated by taking the derivative of Eq. (5) [36]. It should be noted  
354 that this expression is only correct if no transverse magnetization remains before the next RF pulse;  
355 otherwise residual transverse magnetization interferes with longitudinal magnetization and  
356 contributes to the steady state.

357 Whatever the value of  $\beta$ , the  $T_1$  values of signals from different chemical groups differ. Eq. (6) gives  
358 the percentage deviation  $E$  which characterizes the error due to partial saturation:

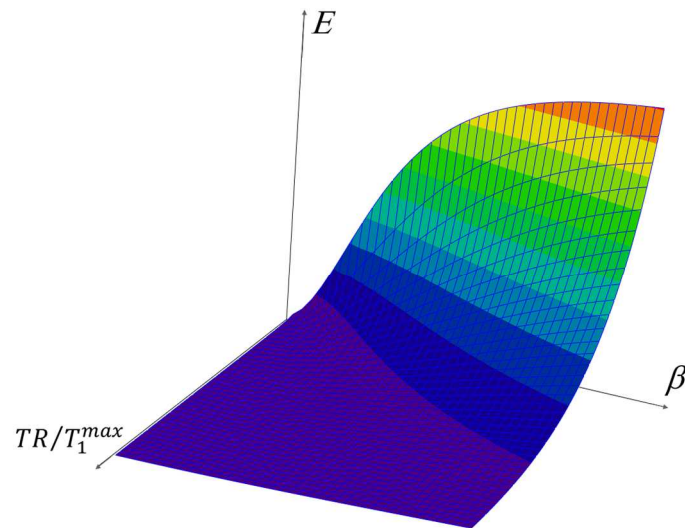
$$359 \quad E = 100 \cdot \frac{e^{-\frac{TR}{T_1} \cdot (1 - \cos(\beta))}}{1 - \cos(\beta) \cdot e^{-\frac{TR}{T_1}}} \quad (6)$$

360 Trueness is then limited by  $E$  obtained for the longest  $T_1$  ( $T_1^{max}$ ).

361 For a given value of  $E$ , one obtains an infinity of couples  $(\beta, TR/T_1^{max})$ , corresponding to the  
362 intersection between the surface represented in **Figure 3** and a horizontal plane. Among these

363 couples, it is now necessary to determine which ensures the best precision. How this is done will be  
364 described in Section 3.4.

365



366

367 **Fig. 3:** Plot of the error  $E$  against the flip angle  $\beta$  and the ratio  $TR/T_1^{max}$ .

368

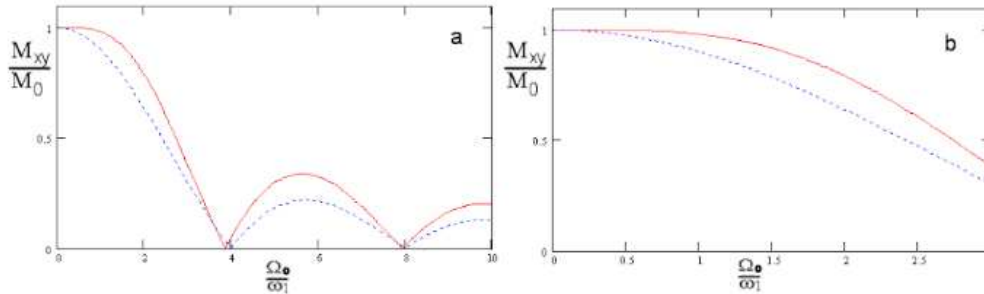
### 369 3.3.2. Off-resonance

370 In the ideal case where the radiofrequency pulse has high power, it is possible to neglect the  
371 precession around  $\vec{B}_0$  during the pulse and to consider that all the magnetizations contributing to the  
372 spectrum undergo - during an RF pulse of duration  $\tau$ - a rotation of angle  $\beta_0 = \omega_1 \cdot \tau$ . This  
373 approximation is frequently made when an accurate analysis is not necessary.

374 However, in many experimental situations, this approximation is not satisfied. In fact, magnetization  
375 precession takes place around an effective field which is not in the transverse plane [36]. The  
376 evolution of  $M_{xy}/M_0$  as a function of  $\Omega_0/\omega_1$  is shown in **Figure 4** for a nominal flip angle of  $\pi/2$ .  
377 Here,  $\Omega_0$  is the signal offset in the rotating frame. It can be seen that  $M_{xy}$  remains close to  $M_0$  as  
378 long as  $\Omega_0$  does not exceed  $\omega_1$ . For larger offsets,  $M_{xy}$  decreases rapidly and even goes through zero.

379 As a first approximation, the evolution of  $M_{xy}$  as a function of  $\Omega_0$  is often described by a sinc  
 380 function. It is therefore reported, for comparison, in **Figure 4**.

381



382

383 **Fig. 4:** Evolution of  $\frac{M_{xy}}{M_0}$  with  $\frac{\Omega_0}{\omega_1}$  from 0 to 10 (a) and from 0 to 3 (b). Dotted lines represent the  $\frac{\sin\left(\frac{\Omega_0 \cdot \tau}{2}\right)}{\left(\frac{\Omega_0 \cdot \tau}{2}\right)}$   
 384 function for comparison.

385

386 This off-resonance effect is another source of error and, for a single-pulse acquisition, trueness is  
 387 therefore limited by the ratio  $M_{xy}/M_0$ . Because this effect depends on resonance frequency, the  
 388 greatest error is observed at the bandwidth edges. For a given error, it is thus possible to calculate  
 389 the maximum permitted bandwidth  $\Delta F^{max}$ . A close examination of the curve plotted in **Figure 4**  
 390 shows that an error of 1% ( $M_{xy}/M_0 = 0.99$ ) is obtained for  $\Omega_0/\omega_1 = 0.84$  which corresponds to  
 391  $\Delta F^{max} = 0.42/\tau_{90}$ , where  $\tau_{90}$  is the duration of a  $\pi/2$  flip angle on resonance. An error of 1‰  
 392 ( $M_{xy}/M_0 = 0.999$ ) is obtained for  $\Omega_0/\omega_1 = 0.46$  and  $\Delta F^{max} = 0.23/\tau_{90}$ .

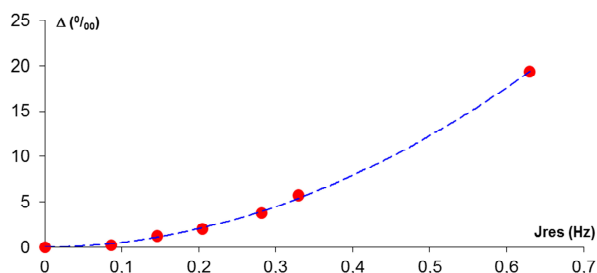
### 393 3.3.3. Heteronuclear decoupling

394 Continuous heteronuclear irradiation, for example during heteronuclear decoupling, induces the  
 395 nuclear Overhauser effect (nOe). Because this effect is not instantaneous and builds up gradually, it is  
 396 possible to avoid its influence on peak areas by using inverse gated decoupling [37]. Theoretical  
 397 descriptions and experimental studies indicate that a long enough repetition time can enable the full  
 398 recovery of the magnetization to its initial value with no nOe [37, 38]: it has been shown that  $TR =$   
 399  $10 \cdot T_1^{max}$  is necessary to reach an accuracy close to 1‰ [39].

400 As will be discussed in Section 3.5, the best results for high-accuracy quantitative NMR are obtained  
401 using lineshape fitting to determine peak areas. However, this is only true when experimental  
402 lineshapes are very close to the theoretical model used (Lorentzian, Gaussian or a combination of the  
403 two).

404 Line shape distortion can notably come from imperfections in heteronuclear decoupling. They can  
405 disperse signal into sidebands, causing signal loss and can leave a residual splitting which is too small  
406 to be resolved but induces deviation of the lineshape from the ideal model, reducing fitting efficiency  
407 and so decreasing trueness (**Fig. 5**) [21].

408



409

410 **Fig. 5:** Impact of the residual coupling  $J_{res}$  (resulting from imperfect  $^1\text{H}$  decoupling) on the trueness of isotopic  
411  $^{13}\text{C}$  NMR measurements.  $\Delta$  is the variation in relative intensities for ethanol. Reprinted with permission from  
412 Ref. [21]. Copyright 2017 Wiley.

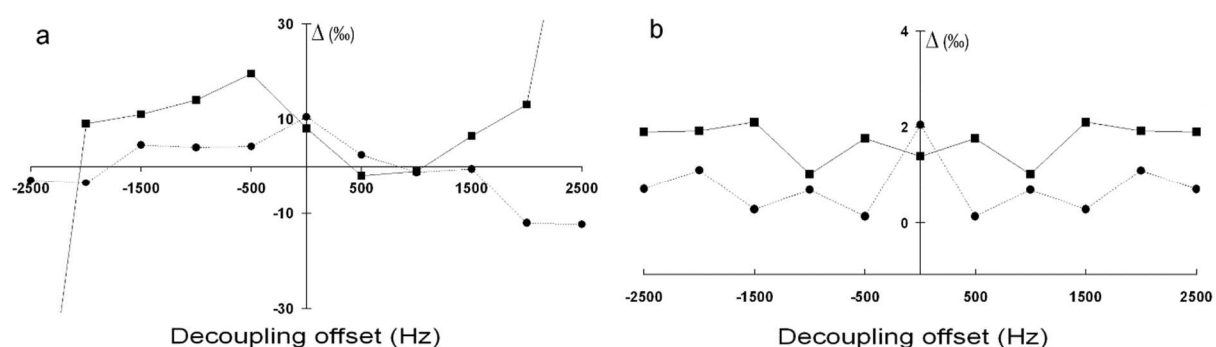
413

414 Furthermore, it has been shown experimentally [40, 41] that composite pulse decoupling schemes do  
415 not allow uniform decoupling over the proton chemical range. This limits trueness to the order of a  
416 few percent.

417 Broadband heteronuclear decoupling has been the subject of numerous studies [42], mainly during  
418 the 1990s. However, these works essentially focused on increasing the width of the decoupled  
419 frequency range. To achieve excellent accuracy over the entire  $^{13}\text{C}$  range, the  $^1\text{H}$  decoupling must be  
420 as uniform as possible. In order to reach this goal, an original approach had to be developed: for each  
421 offset, the minimum adiabaticity factor reached during the pulse was computed, and then the profile

422 obtained was used to optimize the swept frequency range of the adiabatic pulses [41]. This led to  
 423 adiabatic full passage pulses with a cosine amplitude modulation of the RF field ( $\omega_2^{max} = 75.2$  kHz). A  
 424 frequency sweep was performed using the offset independent adiabaticity strategy [43] over an  
 425 optimized bandwidth of 14 kHz and the M4P5–M4P9–M4P50–M4P90 phase cycle was used. As  
 426 shown in **Figure 6**, this resulted in a dramatic improvement in proton decoupling uniformity and so in  
 427 trueness.

428



429

430 **Fig. 6:**  $\Delta$  values (in ‰) as a function of the decoupling offset for the acetic acid molecule (···•··) and for the  
 431 ethanol molecule (-■-). (a) The decoupling was performed using WALTZ-16 with  $\omega_2^{max} = 53.1$  kHz. (b) The  
 432 decoupling scheme used Cos/OIA pulses with  $\omega_2^{max} = 75.2$  kHz. Note the difference in the vertical scale  
 433 between (a) and (b). In this article  $\Delta$  has the same meaning as  $\Gamma$ , defined in section 4.3.2. Reprinted with  
 434 permission from Ref. [41]. Copyright 2007 Elsevier.

435

### 436 3.3.4. Pulse sequence

437 Whatever the sequence used, all the parameters mentioned previously affect trueness, and for some  
 438 of them, such as resonance offset, the effect increases when multi-pulse sequences are used.  
 439 Moreover, in the latter case, transverse relaxation and chemical shift and coupling effects have to be  
 440 added [44].

441 Therefore, the signal of position  $i$  can be written:

442 
$$S_i = k' \cdot \lambda_s \cdot \lambda_n \cdot \lambda_d \cdot \lambda_p \cdot n_i \cdot c \cdot x_i \quad (7)$$

443 where  $\lambda_s$ ,  $\lambda_n$ ,  $\lambda_d$ ,  $\lambda_r$  and  $\lambda_e$  are factors characterizing the effect of partial saturation, nOe,  
 444 heteronuclear decoupling, transverse relaxation and chemical shift and decoupling changes,  
 445 respectively. Clearly, this is not an exhaustive list.

446 **3.4. Parameters influencing precision**

447 **3.4.1. Signal-to-noise ratio**

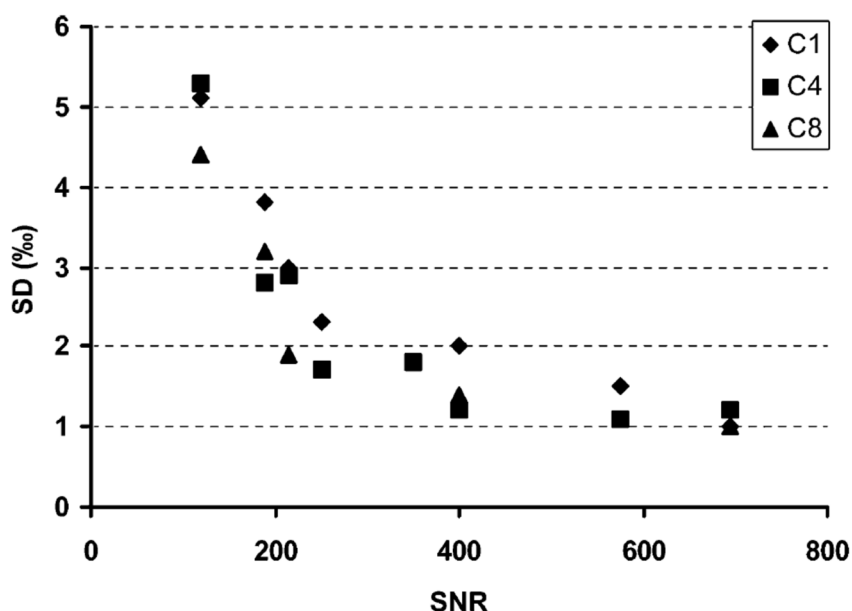
448 The main limit on precision for NMR measurement is the SNR, which can be formalized by [45]:

449 
$$\sigma \leq \frac{1}{2 \cdot SNR} \quad (8)$$

450 where  $\sigma$  is the relative standard deviation of the peak area.

451 This relation was demonstrated experimentally by Caytan *et al.* [14] for isotopic measurements (irm-  
 452  $^{13}\text{C}$  NMR) performed on vanillin samples (**Fig. 7**).

453



454

455 **Fig. 7:** Dependence of the relative standard deviation in permil (‰) on the signal-to-noise ratio (SNR) for three  
 456 carbons of the vanillin molecule (see Fig. 20 carbon numbering). Reprinted with permission from Ref. [14].

457

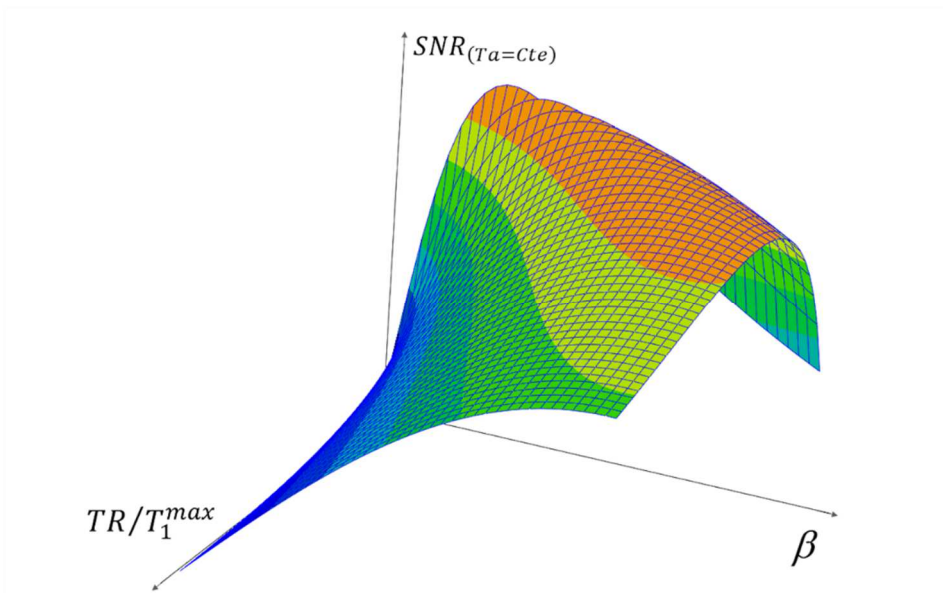


458 Consequently, among the set of couples  $(\beta, TR/T_1^{max})$  described in Section 3.3, it is necessary to  
 459 determine which one ensures the best SNR for a given acquisition analysis time  $T_a$ . It is  
 460 straightforward to demonstrate that:

$$461 \quad SNR_{(Ta=Cte)} = k \cdot \frac{M_{eq} \cdot \sin(\beta)}{\sqrt{TR}} \quad (9)$$

462 where  $SNR_{(Ta=Cte)}$  is the signal-to-noise ratio obtained in a given  $T_a$ .  $SNR_{(Ta=Cte)}$  is plotted in  
 463 **Figure 8** against the ratio  $TR/T_1^{max}$  and the flip angle  $\beta$ .

464



465

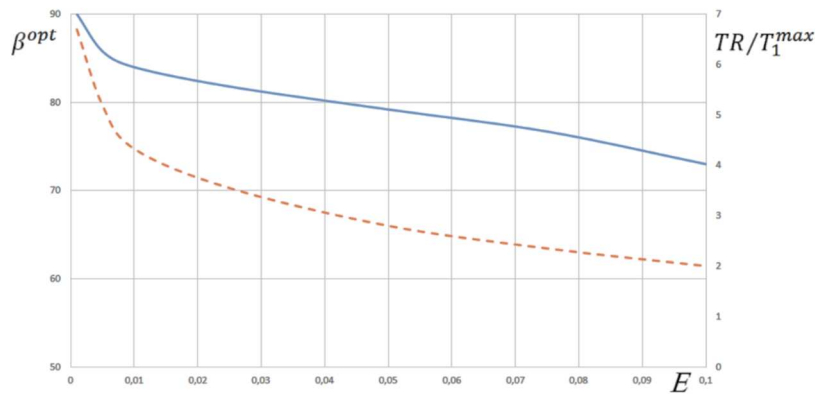
466 **Fig. 8:** Plot of the  $SNR_{(Ta=Cte)}$  against the flip angle  $\beta$  and the ratio  $TR/T_1^{max}$ .

467

468 The intersection between the two sets of couples  $(\beta, TR/T_1^{max})$  (obtained on the basis of trueness  
 469 and precision) provides an optimal couple  $(\beta^{opt}, TR^{opt}/T_1^{max})$ .

470 The optimal flip angle  $\beta^{opt}$  and the optimal ratio  $TR^{opt}/T_1^{max}$  are plotted *versus* the targeted error  
 471 due to partial saturation  $E$  in **Figure 9**. It appears that the more demanding we are of  $E$ , the closer  $\beta$   
 472 is to  $90^\circ$  [37, 38, 39].

473



474

475 **Fig. 9:** Plot of the optimal flip angle  $\beta^{opt}$  (solid line) and the optimal ratio  $TR^{opt}/T_1^{max}$  (dashed line)  
 476 against E, the target value in terms of trueness and precision.

477

478 In addition, as  $\frac{\partial M_{xy}}{\partial \beta}$  is proportional to  $\cos \beta$ , a variation  $\partial \beta$  of the readout pulse produces a variation  
 479  $\partial M_{xy}$  of the magnetization proportional to  $\cos \beta$ . It is therefore for  $\beta$  close to  $90^\circ$  that  $\partial M_{xy}$  will be  
 480 minimum and that  $M_{xy}$  will be less sensitive to some instabilities of the spectrometer. It can be  
 481 concluded that  $\beta = 90^\circ$  ensures maximum robustness of the acquisition.

482 Consequently,  $\beta^{opt} = 90^\circ$  is always a good choice; this leads to  $TR^{opt}/T_1^{max} = 3, 4.6$  and  $7$  for E  
 483 equal to 5%, 1% and 1‰, respectively. Note that when the nOe has to be taken into account,  
 484  $TR^{opt}/T_1^{max} = 10$  has to be chosen (see Section 3.3.3).

### 485 3.4.2. Spectrometer and sample stability

486 Clearly, the stability of the sample plays a big part in the precision obtained and this point has been  
 487 extensively developed in the literature [46-48]. In general, the stability of all parameters influencing  
 488 trueness has a significant impact on precision. This is notably the case for temperature; both that of  
 489 the sample and that of the probe and electronic devices are crucial to obtaining good precision.

490 In addition, all these variations should not only be considered individually. A combination of several  
 491 variations can impact precision more severely than the sum of the effects of each individual  
 492 instability. As an example, RF pulse imperfections cause non-uniform decoupling, which decreases

493 trueness. However, when such imperfections are caused by temperature instability, which also  
494 induces chemical shift variation, it is responsible for the poor precision observed with classic  
495 decoupling schemes [40, 41].

### 496 **3.4.3. Pulse sequence**

497 We mentioned in Section 3.3.4 that the type of sequence influences trueness, but it also has a great  
498 impact on precision. As an example, we have observed that precision obtained with the DEPT  
499 sequence is significantly lower than that obtained with a single-pulse sequence [16, 49].

500 This is mainly due to RF imperfections [44]. However, not all pulses have the same effect: 90° pulse  
501 imperfections reduce all peak areas to the same extent when the off-resonance effect is small [44].  
502 Furthermore, the signal intensity depends on  $\sin\beta$  so a variation in  $\beta$  induces a signal variation  
503 proportional to  $\cos\beta$  [44]. Therefore, the instability of such pulses has a low impact on precision.

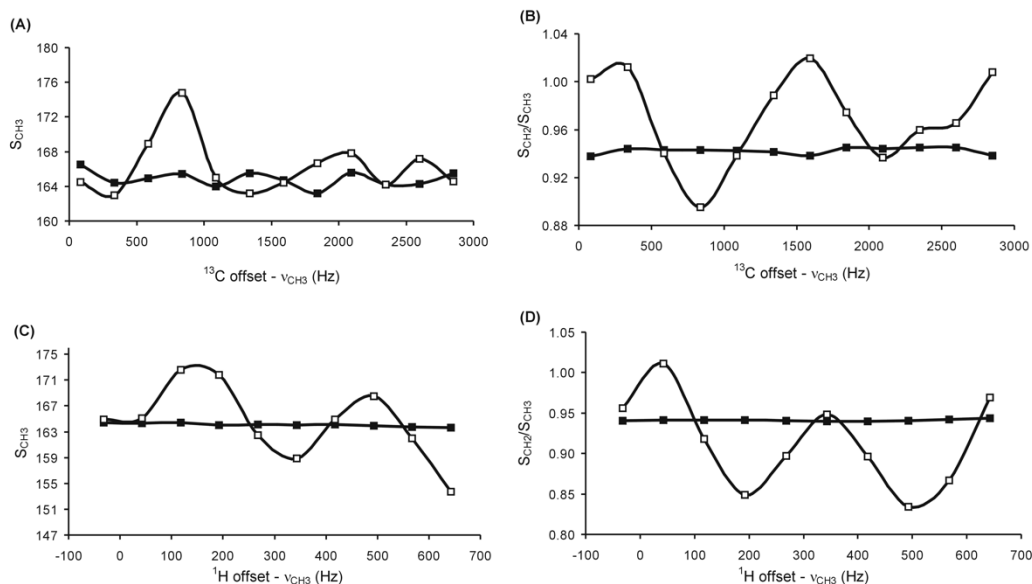
504 On the other hand, 180° pulse imperfections – when they are involved in a spin-echo block – are  
505 responsible for poor refocusing and so have an effect on peak area that depends on the resonance  
506 frequency [44]. Consequently, small temperature variations – that cannot be avoided even with  
507 efficient temperature control – cause a loss in precision. This effect can be overcome by replacing  
508 hard 180° pulses by shaped pulses immune to transmitter variations (such as optimized adiabatic  
509 pulses) [16, 49] (**Fig. 10**).

510 It should be noted that the influence of the sequence on precision can vary greatly from one  
511 sequence to another. We have shown that DEPT reproducibility – even with adiabatic 180° pulses – is  
512 not good enough for  $^{13}\text{C}$  isotopic NMR, while adiabatic INEPT is a powerful tool for such applications  
513 [49]. Moreover, for a sequence like HSQC, the global symmetry in the RF pulse scheme seems to  
514 induce a partial compensation for imperfections, which limits the effect on precision [50].

515 Lastly, relaxation must be taken into account. Multi-pulse sequences include periods of time during  
516 which transverse relaxation induces a decrease in magnetization, especially when the pulse sequence  
517 includes long delays tuned for small, long-range couplings [18]. A small variation in  $T_2$  can therefore

518 generate a variation in peak areas that is not negligible when the target precision is a few permil. This  
 519 imposes severe constraints on the sample preparation protocol, for example the requirement to  
 520 minimize the presence of paramagnetic impurities, including O<sub>2</sub>.

521



522

523 **Fig. 10:** Influence of <sup>13</sup>C and <sup>1</sup>H 180° RF pulse imperfections on the precision of peak areas measured with INEPT  
 524 sequences. For each pulse sequence, the offset was varied systematically over 2750 Hz in steps of 250 Hz (2  
 525 ppm) for <sup>13</sup>C, and over 675 Hz, in steps of 75 Hz (0.15 ppm) for <sup>1</sup>H. Standard INEPT sequence □; adiabatic INEPT  
 526 sequence with composite refocusing pulses (COS/OIA) (▪). (A) Dependence of CH<sub>3</sub> ( $S_{CH_3}$ ) <sup>13</sup>C peak areas in INEPT  
 527 spectra on the difference between <sup>13</sup>C offset and chemical shifts of CH<sub>3</sub>. (B) Ratio  $S_{CH_2}/S_{CH_3}$  of peak areas as a  
 528 function of the difference between the <sup>13</sup>C carrier offset and the chemical shift of the CH<sub>3</sub> group. (C)  
 529 Dependence of CH<sub>3</sub> ( $S_{CH_3}$ ) peak areas in INEPT spectra on the difference between <sup>1</sup>H offset and CH<sub>3</sub> chemical  
 530 shift. (D) Ratio  $S_{CH_2}/S_{CH_3}$  of peak areas as a function of the difference between the carrier <sup>1</sup>H offset and the  
 531 chemical shift of the CH<sub>2</sub> group. Reprinted with permission from Ref. [16]. Copyright 2007 ACS.

532

### 533 3.5. Experimental conditions for high accuracy quantitative NMR

534 From all the considerations mentioned in Section 3, we can derive optimized experimental conditions  
 535 for performing high accuracy quantitative NMR at the level needed for isotopic analysis. The key  
 536 points are: (i) precision is the first objective, and (ii) trueness can be reached by a calibration  
 537 procedure, but only if the  $\lambda_i$  factors of Eq. (7) are reproducible.

538 In this quest for accuracy, temperature plays an important role; it must therefore be strictly  
539 controlled, particularly that of the room and of the sample. Moreover, in most cases, the sample  
540 temperature before it is introduced into the probe differs from the working temperature.  
541 Consequently, there must be a significant stabilization time between sample introduction and the  
542 first instrumental adjustments (probe tuning and matching) [48], in order to ensure that the  
543 temperature is completely stable and homogeneous. As an example, 15 minutes is a minimum  
544 stabilization time for a 5 mm tube introduced at room temperature into a probe regulated at 303 K  
545 and for a sample in water. This time increases with the temperature difference and the tube  
546 diameter and it also depends on what solvent is used.

547 Concerning the influence of longitudinal relaxation and  $nOe$ , they depend strongly on both  
548 temperature and the presence of paramagnetic impurities. Then, it is very difficult to obtain  
549 reproducible values for factors  $\lambda_s$  and  $\lambda_n$ . Therefore, it is essential to eliminate these two  
550 contributions to inaccuracy, as described in Sections 3.3.3 and 3.4.1 [13].

551 As described in Sections 3.3.3 and 3.4.2, high accuracy implies an optimized adiabatic decoupling.  
552 However, the decoupling conditions described in Section 3.3.3 lead to high RF energy deposition [41].  
553 A sampling time of 1 second is thus a good compromise between FID truncation and hardware and  
554 sample safety. Furthermore, the probe geometry is an important parameter for efficient decoupling.  
555 Inverse probes must not be used for X-nucleus acquisition since the proton coil, located as closely as  
556 possible to the sample, is shorter than the X ( $^{13}\text{C}$ ,  $^{15}\text{N}$  or  $^{17}\text{O}$ ) coil. In such a configuration, some of the  
557 X nuclei are not correctly decoupled, which induces distortions in lineshape [51].

558 Multi-pulse sequences can be used and they are a good choice to improve the SNR [16, 49, 50, 52].  
559 However, the type of  $180^\circ$  RF pulses must be carefully chosen and, once again, adiabatic pulses are a  
560 good solution [16, 49]. DEPT must be avoided since it includes an RF pulse that is neither  $90^\circ$  nor  $180^\circ$   
561 – at least if all the carbons bearing proton(s) are measured.

562 Finally, data processing, especially the method used to determine peak areas, is crucial to reach high  
563 accuracy. In the absence of significant signal overlap, integration is the most common approach to  
564 determining peak areas. However, in practice, it often underestimates the areas because of  
565 truncation of the long tails of the Lorentzian lineshape [53]. One of the more important criteria when  
566 choosing the method to measure peak areas is that it must be as independent as possible of the  
567 operator. From this point of view, the best solution is to perform a fit of the experimental data with a  
568 theoretical model (*e.g.* Lorentz-Gauss), which must take many parameters into account so that the  
569 areas under the peaks are determined with great precision. This adjustment must be made at least  
570 on the position, width and intensity, but this is generally not enough to reach a few permil [31]. Shim  
571 imperfections generate broadening and distortions in lineshape. A contribution of Gaussian and  
572 asymmetry must therefore be incorporated into the model. Asymmetry in lineshape is allowed for by  
573 introducing a term in the first derivative of the Gaussian contribution into the lineshape model [54].  
574 From our experience, an error of only 5% in the Gaussian percentage can induce a bias of 10% in the  
575 area determined. Taking into account the peak phases is also crucial since it is impossible to phase  
576 heteronuclear spectra perfectly with a correction of order one. We have found that a four-degree  
577 phase shift (invisible to the naked eye) causes a few permil error in the peak area. In addition, the  
578 baseline must be corrected very carefully, which is difficult to do on the complete spectrum. The best  
579 option is to integrate it into the line-fitting, which must thus be adjusted for each line: position,  
580 width, intensity, phase, Gaussian %, asymmetry and baseline [31, 55]. This adjustment can be made  
581 in the time domain or in the frequency domain.

582

## 583 **4. Isotope ratio measurement by NMR**

### 584 **4.1. Isotopic fingerprinting**

585 The determination of molar fractions  $f_i$  using Eq. (4) is sufficient to measure the relative contents of  
586 the different isotopomers if it is carried out with high precision (% for  $^2\text{H}$  and ‰ for  $^{13}\text{C}$  or  $^{15}\text{N}$ ). For  
587 authentication applications, trueness is not an issue and the molar fraction profile is thus sufficient to  
588 obtain an isotopic fingerprint. Moreover, in such cases, it is not always essential to measure the  
589 isotope content of all the positions [56] and intensity distortions induced by multi-pulse sequences  
590 are not drawbacks [49, 57], even in 2D [50, 52] (see Section 5). As an example, in the case of the  
591 INEPT sequence, the transfer of polarization leads to an increase in sensitivity up to a factor of four  
592 and a gain is also achieved by shortening the  $TR$ , since it is now governed by the  $^1\text{H}$   $T_1$  values, which  
593 are significantly smaller than those of  $^{13}\text{C}$ .  $TR$  can be set at the value of seven times the proton  
594  $T_1^{max}$ , which contributes to decreasing the analysis duration.

### 595 **4.2. Position-specific isotope abundance measurement**

596 As mentioned in the previous Section, molar fractions  $f_i$  only give the relative contents of the  
597 different isotopomers. Two methods can be used to obtain absolute position-specific isotope  
598 abundances ( $x_i$ ).

#### 599 **4.2.1 Using average isotope abundance**

600 If the average isotope abundance of the entire molecule ( $x_g$ ) is known, specific isotope abundances  
601 ( $x_i$ ) can be calculated using Eq. (10).

$$602 \quad x_i = x_g \cdot \frac{f_i}{F_i} \quad (10)$$

603 where  $F_i$  is the statistical molar fraction (*i.e.* without any isotope fractionation);  $F_i = n_i / \sum n_i$  with  $n_i$   
604 the number of equivalent nuclei at the position  $i$ .

605  $x_g$  is determined using irm-MS, so this method requires the use of two different analytical  
606 techniques: NMR and mass spectrometry. Furthermore, it can only be used when the molar fractions  
607 of all sites are measured [31].

#### 608 4.2.2. Using an isotopic internal reference

609 The  $x_i$  values can also be obtained by using an internal reference of known isotope abundance [58].

$$610 \quad x_i = x_{ref} \cdot \frac{S_i}{S_{ref}} \cdot \frac{n_{ref}}{n_i} \cdot \frac{c_{ref}}{c} \quad (11)$$

611 where  $x_{ref}$  is the isotope abundance of the reference compound;  $S_{ref}$  is the peak area of the  
612 reference compound;  $n_{ref}$  is the number of equivalent hydrogens associated with the reference;  $C$  is  
613 the molar concentration of the measured compound and  $C_{ref}$  the molar concentration of the  
614 reference compound.

615 The basic way to determine the molar ratio  $C_{ref}/C$  is to use gravimetry:

$$616 \quad \frac{c_{ref}}{c} = \frac{m^{ref} \cdot p_m^{ref}}{m \cdot p_m} \cdot \frac{M}{M^{ref}} \quad (12)$$

617 Here,  $m$  and  $M$  are the weights used for the NMR tube preparation and the molar mass, respectively,  
618 and  $p_m$  is the mass purity.

619 This approach is effective for  $^2\text{H}$  because the required precision is only of the order of a percent, but  
620 it turns out to be extremely delicate for  $^{13}\text{C}$  or  $^{15}\text{N}$  because the precision is then of the order of a few  
621 permil.

622 The second way to determine the molar ratio is to use  $^1\text{H}$  NMR [59].

$$623 \quad \frac{c_{ref}}{c} = \frac{S_{1H}^{ref} \cdot n_{Hi}}{S_{1Hi} \cdot n_H^{ref}} \quad (13)$$

624 With this approach, all the data are obtained with NMR without need of another method. Moreover,  
625 if there are no overlaps between the signals being analyzed and signals from any impurities that may  
626 be present, then it is no longer necessary to know purities. In addition, it is no longer essential to  
627 measure all the sites and thus multi-pulse sequences can be used as long as specific factors ( $\lambda_i$ ) are



628 determined by comparison with data from single-pulse acquisitions (this last point is currently being  
629 validated in our laboratory).

630 However, to measure  $^{13}\text{C}$  NMR spectra with high precision, a high SNR and thus high concentrations  
631 are necessary. If the proton spectrum is acquired from the same sample as for the  $^{13}\text{C}$  spectrum, the  
632 former may be corrupted by radiation damping, which is incompatible with high accuracy  
633 measurement.

634 This last drawback can be overcome by specific methods. We have shown that accurate  $^1\text{H}$   
635 quantitative NMR can be performed on concentrated samples by suppressing most of the signal and  
636 keeping only that coming from a thin slice in the center of the sample [60, 61].

#### 637 **4.2.3. Correction for contribution of bi-labeled isotopologues**

638 Before applying Eqs. (10) or (11) to calculate isotope abundances, peak areas must be corrected to  
639 take into account the contribution of bi-labeled isotopologues [62]. This can be disregarded for  $^2\text{H}$   
640 because of its low natural abundance, but not for  $^{13}\text{C}$ . The isotopologues bearing a  $^{13}\text{C}$  at position  $i$   
641 include mono-labeled isotopologues (one  $^{13}\text{C}$  at position  $i$  and only  $^{12}\text{C}$  at other positions) and multi-  
642 labeled isotopologues (one  $^{13}\text{C}$  at position  $i$  and  $^{13}\text{C}$  at other positions). Isotopologues with more than  
643 two  $^{13}\text{C}$  are too scarce to make a significant contribution, but bi-labeled isotopologues generate  
644 doublets (satellite lines). When the two  $^{13}\text{C}$  are separated by at least two bonds, satellites are  
645 included in the peak tails and these isotopologues contribute to the area of the main line (see **Fig. 2**).  
646 However, when the two  $^{13}\text{C}$  are at adjacent positions, the satellite lines are well resolved because the  
647  $^{13}\text{C}$ - $^{13}\text{C}$  scalar coupling values are large. Because of their SNR, it is not possible to quantify these  
648 satellite lines with high accuracy, but they can be taken into account using Eq. (14).

$$649 \quad S_i = S'_i (1 + u \times 0.011) \quad (14)$$

650 Here,  $S'_i$  is the area under the main peak,  $u$  is the number of carbons linked to position  $i$ , 0.011 is the  
651 average natural isotope abundance of  $^{13}\text{C}$  and  $S_i$  is therefore proportional to the total number of  $^{13}\text{C}$   
652 located at position  $i$ .

653

#### 654 4.2.4. Partial, apparent and true isotopic composition

655 The isotopic compositions measured by the single-pulse methodology (with inverse gated adiabatic  
656 decoupling) are expected to be the “true” values. This is almost always the case for standard NMR  
657 spectrometers, as shown by the ring test performed on similar instrumental configurations (400 MHz  
658 and BB or dual  $^{13}\text{C}/^1\text{H}$  probes) from which an inter-machine standard deviation lower than 2‰ was  
659 found [51]. Furthermore, the  $\delta^{13}\text{C}_i$  values were very similar to those found by other PSIA methods  
660 such as pyrolysis coupled to irm-MS [63]. Nonetheless, significant variations were found in relation to  
661 the range of the chemical shifts: the extreme side peaks of the spectrum showed the largest  
662 discrepancies [64]. This divergence is accentuated by using cryoprobes at very high fields. “True”  
663 values would be obtained by applying correction factors, depending on the spectrometer response  
664 after measuring international standards, from which a consensus on the intramolecular  $^{13}\text{C}$   
665 distribution could be established. Work is in progress to select molecules, such as alanine [65], that  
666 could fit these requirements.

667 When multi-pulse sequences such as INEPT are used, polarization transfer is commonly achieved  
668 using  $^1\text{J}_{13\text{C}-1\text{H}}$  couplings. As a result, the quaternary carbons are not observed. The  $^{13}\text{C}$  profile is  
669 therefore partial. In addition, the intensity of the signal is affected by the values of transfer and  
670 refocusing delays, that is to say that the  $\lambda$  coefficients of Eq. (7) are not the same for all the detected  
671 peaks. Areas are not solely proportional to the number of nuclei but also depend on the sequence  
672 parameters. Therefore, the measured  $f_i$  values are partial and apparent as they are not the true  
673 molar fractions of all isotopomers. The only parameters that can provide a full statistical distribution  
674 are therefore these partial fractions  $f_i$  or  $f_i / F_i$ . When the number of quaternary carbons is relatively  
675 small compared to the protonated carbons, the partial profile, *i.e.* with the protonated carbons only,  
676 is usually enough for effective discrimination between samples. The resulting partial intramolecular  
677 distribution leads to profiles that could be used as input data for -omics interpretation (isotopomics).  
678 The calculation of the position-specific  $^{13}\text{C}$  isotope composition  $\delta^{13}\text{C}_i$  cannot be performed as is done

679 for the single-pulse experiment, for which the full  $^{13}\text{C}$  distribution can be retrieved relatively from the  
680 global  $^{13}\text{C}$  content (measured by irm-MS, for example, see Section 4.2.1) once all area signals have  
681 been deconvoluted. Eq. (10) cannot be used because it requires all the peaks to be measured. The  
682 conversion to  $\delta^{13}\text{C}_i$  would be possible from the internal reference by calculating the apparent isotopic  
683 composition of the available isotopomers. As discussed above, correction factors could then be  
684 applied to express these  $\delta^{13}\text{C}_i$  on a consensual international  $\delta$ -scale.

685 In some cases, the number of quaternary carbons is not negligible and information is missing, as  
686 illustrated by the study of the origin of caffeine (see Section 5). The delay for the transfer of  
687 polarization in INEPT can be adjusted to the long-range  $^1\text{H}$ - $^{13}\text{C}$  couplings ( $^n\text{J}_{13\text{C}-1\text{H}}$ ). However,  
688 adaptations were required in order to reach the targeted precision, and matched transfer and  
689 refocusing delays were found [18].  $|^n\text{J}_{13\text{C}-1\text{H}}|$  can range from 0 to 20 Hz, leading to spin-echo periods  
690 longer than 100 ms in total. The loss of signal via transverse relaxation cannot be neglected: one has  
691 to be sure that the signal attenuation caused is always the same, whatever the sample or the  
692 experiment, for a given molecule. Robustness is ensured by fixing the acquisition parameters and the  
693 sample preparation. The resulting methodology was named Full-Spectrum INEPT (FS-INEPT) [18]. It  
694 was shown that the full  $^{13}\text{C}$  profiles could be obtained with 40 mg of caffeine or acetaminophen in a  
695 short time (see Section 5). This strategy was also tested for  $^{15}\text{N}$  profiling, since several (bio)organic  
696 nitrogen-containing molecules do not exhibit  $^1\text{J}_{15\text{N}-1\text{H}}$  couplings, providing long-range couplings only.  
697 In these cases, all the peaks are measured and apparent isotope compositions are obtained once  
698 again [19]. Eq. (11) leads to apparent isotope compositions  $\delta^{13}\text{C}_i$  or  $\delta^{15}\text{N}_i$  that are meaningless, *i.e.* are  
699 not expressed on the absolute scale from the international standard V-PDB for  $^{13}\text{C}$  or from  
700 atmospheric  $\text{N}_2$  for  $^{15}\text{N}$ , as obtained by irm-MS ( $\delta^{13}\text{C}_g$  and  $\delta^{15}\text{N}_g$ ) or even from an internal reference.  
701 As mentioned above, to retrieve the true isotopic compositions, appropriate calibration has to be  
702 performed, by comparing the values obtained on a reference sample of the given molecule with the  
703 single-pulse sequence and with the multi-pulse sequence, leading to suitable correction factors.  
704 However, even when only apparent isotope compositions are obtained, the variations between

705 samples are on the same scale as irm-MS: if  $\Delta\delta_i$  is defined as the change in isotopic composition  
 706 between samples, it is then as correct as  $\Delta\delta_g$  (obtained by irm-MS) even if  $\delta_i$  is not on the  
 707 standardized scale. The extent of  $\Delta\delta_i$  can be directly compared to  $\Delta\delta_g$  since they are expressed on the  
 708 same relative scale with similar precision.

### 709 **4.3. Practical aspects**

#### 710 **4.3.1. $T_1^{max}$ measurement**

711 As discussed in Section 3, knowledge of the greatest longitudinal relaxation time ( $T_1^{max}$ ) is necessary  
 712 to establish optimal conditions for high accuracy NMR.

713 Saito *et al.* [45] showed that the target accuracy for the area determination ( $\xi_s$ ) is linked to the  
 714 accuracy of the  $T_1^{max}$  determination ( $\xi_{T_1}$ ) by Eq. (15).

$$715 \quad \xi_s = \sqrt{\left(\frac{\partial S}{\partial T_1}\right)^2 \cdot \xi_{T_1}^2} \quad (15)$$

716 which means that, whatever the  $\xi_s$  value, 10% is sufficient for  $\xi_{T_1}$  [45].

717 In order to obtain the best dynamic range, the inversion-recovery sequence must be used with the  
 718 first inversion time ( $TI$ ) close to zero and the last  $TI$  equal to five times the expected value for  $T_1^{max}$   
 719 [66].

720 Regarding the values and distribution of  $TI$ , we have evaluated three strategies. Montecarlo  
 721 simulations were done using 4, 6, 8 and 16 values of  $TI$  ranging from 5 ms to  $5 \cdot T_1^{max}$  and distributed  
 722 following an arithmetic progression, a geometric progression, or a distribution assuring the  
 723 arithmetic progression of  $M_z$  (Eq. (16)).

$$724 \quad TI_k = -T_1^{expt} \cdot \text{Ln} \left(1 - \frac{k}{N}\right) \quad (16)$$

725 where  $N$  is the number of  $TI$  values,  $T_1^{expt}$  is the expected value for  $T_1^{max}$ , and  $k$  ranges from 0 to  $N$ .

726 The  $TI$  value giving  $M_z = 0$  is omitted.

727 This last strategy with  $N = 6$  gives the best accuracy for  $T_1$  when simulations are performed at a  
728 constant SNR and constant experimental time.

729

### 730 4.3.2. Spectrometer performance evaluation

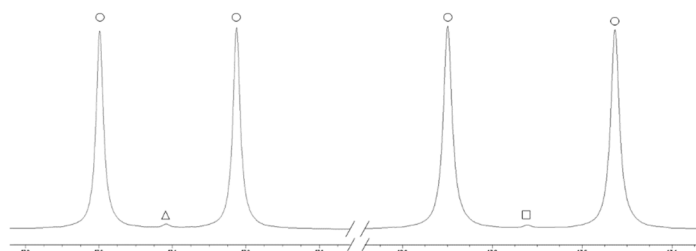
731 The success of high accuracy quantitative NMR is greatly dependent on hardware specifications and  
732 stability. It is therefore essential to evaluate the spectrometer performance in terms of trueness and  
733 precision on a standard sample. However, it is not easy to obtain a sample with several chemical  
734 shifts and known specific natural isotope abundances, since NMR is the only method that can  
735 measure this. To address this problem, we have proposed using bi-labeled two-carbon molecules  
736 such as  $^{13}\text{C}$ -1,2-ethanol or  $^{13}\text{C}$ -1,2-acetic acid [13, 40].

737 **Figure 11** shows the  $^{13}\text{C}$  NMR spectrum of  $^{13}\text{C}$  bi-labeled ethanol. The  $^{13}\text{CH}_3^{13}\text{CH}_2\text{OH}$  isotopologue  
738 gives rise to two doublets, due to  $^{13}\text{C}$ - $^{13}\text{C}$  scalar coupling, while the  $^{12}\text{CH}_3^{13}\text{CH}_2\text{OH}$  and  $^{13}\text{CH}_3^{12}\text{CH}_2\text{OH}$   
739 isotopologues generate one singlet each. There is no overlapping of these six lines and so it is easy to  
740 quantify the peaks of the bi-labeled isotopologue without interferences.

741 This isotopologue plays the role of the standard molecule. In the absence of instrumental  
742 imperfections, the areas of the two doublets are identical, regardless of the real  $^{13}\text{C}$  abundance of  
743 each site of bi-labeled ethanol. Thus, the ratio of the  $^{13}\text{CH}_2$  doublet area to the  $^{13}\text{CH}_3$  doublet area is  
744 exactly equal to 1.000. This can be evaluated experimentally using the parameter  $\Gamma$  ( $\%$ ) defined by  
745 Eq. (17) [13].

$$746 \quad \Gamma (\%) = \left( \frac{f_{\text{CH}_2}}{F_{\text{CH}_2}} - 1 \right) \times 1000 = \left( \frac{f_{\text{CH}_2}}{0.5} - 1 \right) \times 1000 \quad (17)$$

747



748

749 **Fig. 11:** Proton decoupled  $^{13}\text{C}$  NMR spectrum of  $^{13}\text{C}$  bi-labeled ethanol. ( $\circ$ ) Peaks due to the  $^{13}\text{CH}_3^{13}\text{CH}_2\text{OH}$   
750 isotopologue, ( $\Delta$ ) peak due to the  $^{12}\text{CH}_3^{13}\text{CH}_2\text{OH}$  isotopologue and ( $\square$ ) peak due to the  $^{13}\text{CH}_3^{12}\text{CH}_2\text{OH}$   
751 isotopologue.

752  $^{13}\text{C}$ -1,2-ethanol and  $^{13}\text{C}$ -1,2-acetic acid are commercially available and are each of interest for specific  
753 reasons. Acetic acid is used to evaluate the impact of a broad  $^{13}\text{C}$  chemical range, and ethanol to take  
754 into account the impact of proton-proton homonuclear scalar coupling. Studies with these two  
755 molecules have established the experimental conditions required to obtain the high trueness and  
756 precision needed by irm-NMR [13, 14, 41]. They are also an essential element in evaluating a  
757 spectrometer before using it for isotopic NMR [51].

758

## 759 **5. Applications**

760 There are many varied fields in which the isotope ratios for  $^{13}\text{C}$  or  $^{15}\text{N}$  are used: ecology, archeology,  
761 planetology, geosciences, forensic research, metabolism, environment/climate change and  
762 authenticity/counterfeiting, to name the major applications. The previous Sections described how to  
763 perform irm-NMR and obtain the precision required. In this Section, we present typical and relevant  
764 applications of irm-NMR, mainly using  $^{13}\text{C}$  in three areas: detection of counterfeiting, forensic  
765 investigations, and authenticity in food. The reader will find other specific contributions in the  
766 relevant literature ([67-69] for example). Finally, new applications have been found in -omics  
767 approaches. We begin with a paragraph on sample preparation, the goal of which is not to describe  
768 the specific procedure that can be found in each cited reference, but rather to focus on the general  
769 nature of the sample introduced into the NMR tube.

### 770 **5.1. Sample preparation**

771 We believe that the analyst should take care not only of the NMR parameters, as described above,  
772 but also of the sample that will be introduced into the NMR tube. The extraction and purification of  
773 the molecule to be studied must retain the isotopic integrity as it was in the matrix. Some typical  
774 preparation steps have been identified as potential sources of fractionation, while others can be  
775 used safely. We focus on the main ones, such as distillation and chromatography, as well as on  
776 derivatization. It is worth noting that intramolecular isotopic determination by irm-NMR reveals  
777 effects that irm-MS cannot detect. As such, the examples described below contribute to illustrating  
778 the interest of irm-NMR.

#### 779 **5.1.1. Distillation**

780 During the liquid-vapor transition, molecules remaining in the liquid phase undergo a  $^{13}\text{C}$  depletion as  
781 the distillate is  $^{13}\text{C}$ -enriched, while it is the opposite for  $^2\text{H}$  and  $^{18}\text{O}$  (the light isotopologue distills  
782 first), as shown by irm-MS [70]. PSIA by irm- $^{13}\text{C}$  NMR reveals a clear trend between the  $^{13}\text{C}$   
783 enrichment factors of the carbon bearing the heteroatom of chemical functions, upon distillation

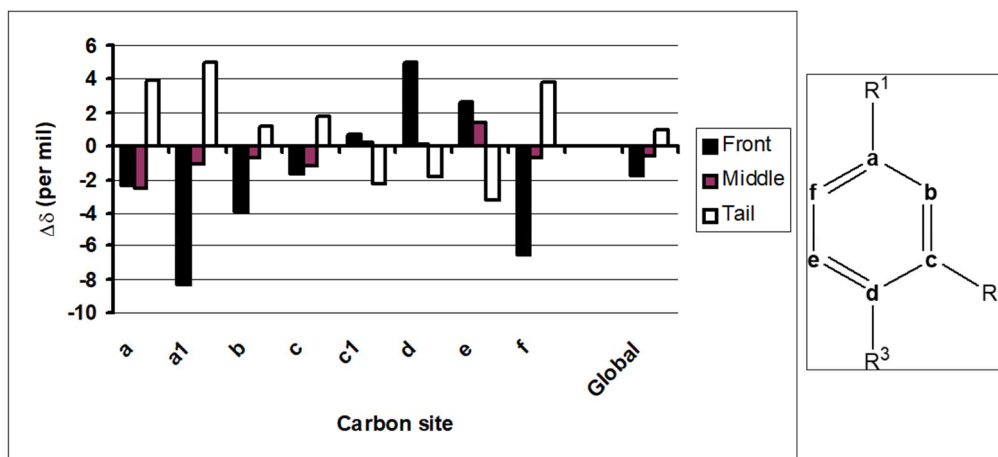


784 [71]. The enrichment/depletion is strongly linked to the relative permittivity, the solvent hydrogen-  
 785 bond acidity, and the solvent hydrogen-bond basicity [72]. If the recovering ratio of the target  
 786 molecule is relatively low, the isotope fractionation could be significant, with an isotope profile that  
 787 would depend on the fraction collected, *e.g.* the product of interest is in the distillate or remains in  
 788 the tail.

### 789 5.1.2. Chromatography

790 During elution on silica gel (normal phase) as the stationary phase, the first fraction collected shows a  
 791 globally impoverished heavy isotope content, as found for  $^2\text{H}$ ,  $^{13}\text{C}$  and  $^{18}\text{O}$  of vanillin during the  
 792 purification step [73]. Furthermore, the position-specific isotope compositions show a dependence  
 793 on the position and functionality of the substituents present. Such non-covalent isotope effects are  
 794 hidden when only the global  $^{13}\text{C}$  content is measured by mass spectrometry since they can be normal  
 795 or inverse and vary with the substitution pattern present, as illustrated by **Figure 12** [73].

796



797

798 **Figure 12:** Position-specific fractionation of  $^{13}\text{C}$  of vanillin during normal phase silica gel column

799 chromatography determined by irm- $^{13}\text{C}$  NMR. The relative variation in  $^{13}\text{C}/^{12}\text{C}$  is expressed as

800  $\Delta\delta_i = (\delta_{\text{eluted}} - \delta_{\text{initial}})_i$  for each carbon position  $i$  of the eluted vanillin ( $\delta_{\text{eluted}}$ ) $_i$  with respect to the initial value

801 measured for site  $i$  ( $\delta_{\text{initial}}$ ) $_i$ . The numbering of each isotopomer for vanillin is for  $\text{R}_1 = \text{CHO}$ ,  $\text{a}_1$ ,  $\text{R}_2 = \text{OCH}_3$ ,  $\text{c}_1$

802 and  $\text{R}_3 = \text{OH}$ . The data presented are from the first collected fraction (from 0 to 11%), the middle fraction (from

803 28 to 33%) and the last eluted fraction (tail = from 76 to 100%). Global is the total <sup>13</sup>C mean value for each of  
804 these portions determined by irm-MS. Adapted from [73].

805 This step is therefore a source of isotope fractionation that can be minimized via a high recovery  
806 yield (> 90%), and evaluated by determining the fractionation on the working standard on which the  
807 protocol was developed [74].

### 808 **5.1.3. Miscellaneous**

809 Extraction is often the first step required to purify the molecule of interest, by two main ways,  
810 distillation and preparative chromatography. It has been shown that both solid-liquid and liquid-  
811 liquid extraction, as well as recrystallization, do not generate isotope fractionation [74, 75]. Irm-NMR  
812 encounters the problems found in any analytical method *i.e.* the fact that analyte molecules may in  
813 general have non-ideal solubility, stability or overlapping signals. In this case, derivatization is often  
814 the preferred solution. Once again, great care should be taken to ensure the conversion yield is >  
815 90%, to avoid significant isotope fractionation. Derivatization must be shown to lead to no, or at least  
816 a reproducible, isotope effect. As an illustration, this was well demonstrated in the study of glucose  
817 and fructose [76] and of xanthines [77] (see Section 5.4.1). Generally speaking, these purification  
818 steps should always be included in the validation of the method, in order to confirm that the isotope  
819 profile is relevant for interpretation.

### 820 **5.2. Counterfeiting**

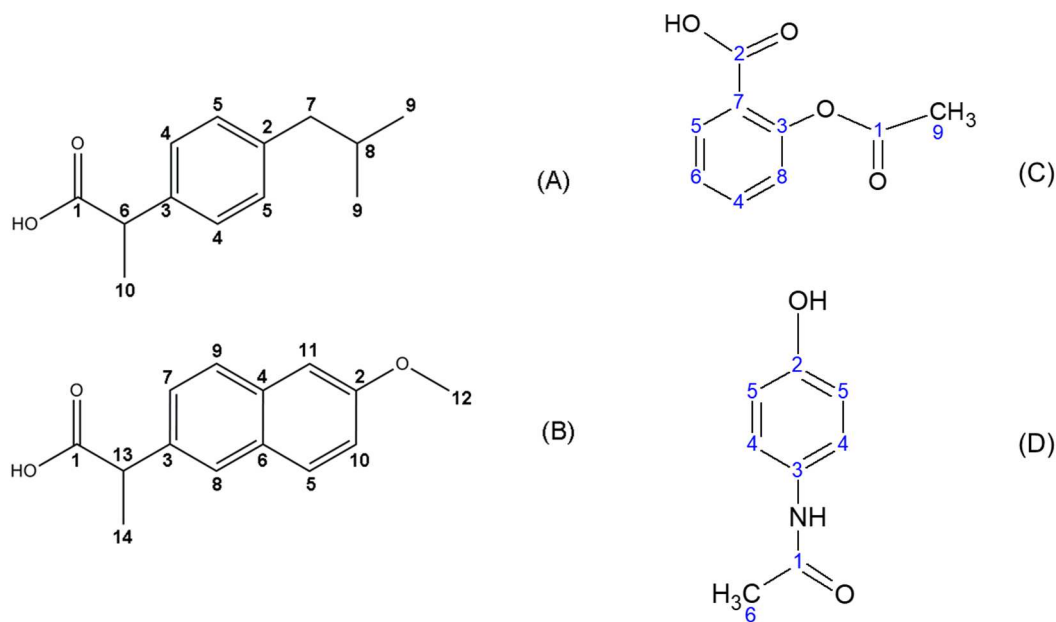
821 The word “counterfeit” is now usually defined by and associated with the protection of intellectual  
822 property rights. On 29 May 2017, at the Seventieth World Health Assembly [78], a decision was made  
823 to adopt the term “Substandard and Falsified (SF) medical products”. The WHO proposed that “in the  
824 context of medical products, the term “falsified” appears to adequately include all the various types  
825 of deliberate misrepresentation of a medical product in such a way which enables the specific  
826 exclusion of intellectual property rights”. Testing how an active molecule was made can be useful for  
827 detecting sophisticated fraudulent practices such as (i) deliberate copying of existing patents for

828 processes or formulations; (ii) stolen and relabeled drugs; and (iii) trans-shipment of goods. Isotopic  
829 approaches are the most efficient because the molecule itself is the object of the study. Classic  
830 analytical tools (chromatography, mass spectrometry, *etc.*) can be used to detect the chemical  
831 impurities generated from the synthesis processes used, such as the remaining raw materials,  
832 intermediates and residual solvents [79]. Nonetheless, these have their limitations. Irm-MS was the  
833 first isotopic method employed and was found to be particularly valuable for distinguishing batches  
834 [80]. However, there is only one parameter per element ( $\delta_g$ ). Thus, even if a multi-element study is  
835 undertaken, the number of parameters that can be used to discriminate between batches or origins  
836 is still restricted to five for the common isotopes ( $^2\text{H}$ ,  $^{13}\text{C}$ ,  $^{15}\text{N}$ ,  $^{18}\text{O}$ ,  $^{34}\text{S}$ ), depending on the atomic  
837 composition [81]. In contrast, irm-NMR will provide as many parameters as isotopomers detected,  
838 *e.g.* 10 parameters for a molecule containing 10 carbons by irm- $^{13}\text{C}$  NMR, thus creating a unique tag  
839 [82]. We describe here the application of irm-NMR to several APIs, highlighting the different  
840 methodologies that can be used according to the type of API.

841 Twenty samples of aspirin and sixteen samples of acetaminophen were bought from pharmacies in  
842 several countries and then submitted to irm- $^{13}\text{C}$  NMR after purification of the active molecules [83].  
843 Nine  $^{13}\text{C}$  isotopomers can be observed for acetylsalicylic acid corresponding to the nine different  
844 carbons of the molecule (**Fig. 13**), and six  $^{13}\text{C}$  isotopomers can be observed for the eight carbons in  
845 acetaminophen due to the symmetry of the aromatic ring (**Fig. 13**). The single-pulse method was  
846 applied, leading to  $^{13}\text{C}$  NMR spectra with all peaks sufficiently resolved for adequate area  
847 measurement. The position-specific  $^{13}\text{C}$  composition values -notably in the substituent groups-  
848 exhibit significant inter-sample variations. The origin of the acetate/acetic acid used (biological or  
849 fossil) displays a large variation for both positions (C1 and C9 for acetylsalicylic acid; C1 and C6 for  
850 acetaminophen), within the range usually observed for acetic acid synthesized from natural gas and  
851 petrochemical sources on one hand and from a biological source, *e.g.* vinegar, on the other hand. As  
852 a non-predictive tool, principal component analysis (PCA) is well adapted for studying data obtained  
853 from a relatively small number of samples with a relatively large number of variables (at least > 3).

854 For both aspirin and acetaminophen, each sample has its own position in a 2D PCA plot (PC1 versus  
855 PC2), illustrating that the  $^{13}\text{C}$  profile is unique for each product [83]. It is also clear that proximity  
856 between samples indicates that they are from similar origins.

857



858

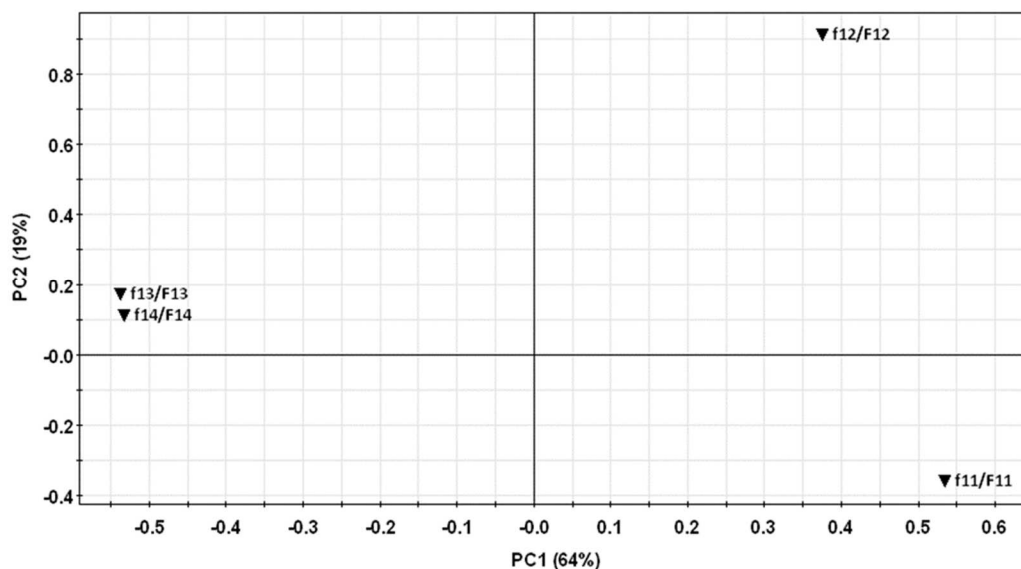
859 **Figure 13:** Molecular structure of ibuprofen (A), naproxen (B), acetylsalicylic acid (C) and acetaminophen (D)  
860 with the carbon atoms numbered in relation to the decreasing  $^{13}\text{C}$  chemical shift in the  $^{13}\text{C}$  NMR spectrum. This  
861 numbering is very convenient to identify easily each isotopomer from its chemical shift according to its  
862 electronic environment. In order to help readers that are not familiar to this notation, the numbered structure  
863 is linked to each NMR spectrum in the following.

864

865 The intrinsically low sensitivity of single-pulse  $^{13}\text{C}$  NMR is still an issue for larger or less soluble  
866 molecules, as illustrated for ibuprofen and naproxen [84]. The irm- $^{13}\text{C}$  INEPT NMR spectra of  
867 ibuprofen and naproxen were obtained in a short time. As the polarization transfer occurs via the  
868 one-bond coupling  $^1J_{^{13}\text{C}-^1\text{H}}$ , the quaternary carbons are missing. In this work, 11 samples of naproxen  
869 and 20 samples of ibuprofen were collected [84]. As discussed previously,  $^2\text{H}$  NMR experiments on  
870 naproxen do not lead to useful data, even when the naproxen is esterified [85]. The global value  $\delta^{13}\text{C}_g$

871 for both products spans a range with no clear clusters. The isotopic INEPT experiment introduces  
872 nine new parameters ( $f_i/F_i$ ) for naproxen and seven for ibuprofen (Fig. 13).

873



874

875 **Figure 14:** Loading plots from the PC1 vs. PC2 principal component analysis on naproxen with experimental  
876 parameters used for classification:  $f_{11}/F_{11}$ ,  $f_{12}/F_{12}$ ,  $f_{13}/F_{13}$  and  $f_{14}/F_{14}$  (see Fig 13 for carbon numbering). The

877 further the parameter is located from the center, the more it contributes to the discrimination (based on data  
878 from [84]).

879

880 These factors are the apparent-partial-reduced molar fractions (see Section 4.2). ‘Apparent’ because  
881 the area of the signal is dependent on the delays of the INEPT sequence (but repeatable, once  
882 chosen) and ‘partial’ because the quaternary carbons are not observed. These factors are  
883 meaningless in themselves but their variations between samples are solely due to the change in  $^{13}\text{C}$   
884 distribution within the molecule that is the target of the discrimination study. For an expression of  
885 the results on the  $\delta$ -scale from international standards, a correction could be applied by studying a  
886 product with a known  $\delta^{13}\text{C}_i$ . This stage is not beneficial for detecting counterfeiting: in fact,  $f_i/F_i$  can  
887 be used in a chemometric analysis, leading to an -omics approach (isotopomics concept). A PCA using  
888 these parameters confirms that each sample is distinguished: the individual  $^{13}\text{C}$  profile is a marker of

889 the label origin for each batch (raw material and process). For naproxen, the explained variance of  
890 77% is rather good, indicating that most of the parameters have a discrimination potential. A close  
891 inspection of the data shows that the apparent-partial-reduced molar fractions  $f_{11}/F_{11}$ ,  $f_{12}/F_{12}$ ,  $f_{13}/F_{13}$   
892 and  $f_{14}/F_{14}$  provide the best discrimination (**Fig. 14**). Interestingly, the corresponding carbons are  
893 those most involved in or closest to the reaction sites during synthesis [84].

### 894 **5.3. Forensic investigations**

895 Stable isotope analyses are now an established addition to the set of forensic technologies, as they  
896 can distinguish chemically identical compounds from different sources [86]. The origin of a  
897 contaminant (*e.g.* during a pollution event) or sensitive materials (such as explosives) or drugs is of  
898 great interest to law enforcement agencies. Isotopic profiles provide a great deal of information at  
899 both strategic and tactical levels. Strategic, because often too little is known of the sources and  
900 migration paths of these products. A better understanding of their marketing structure will help  
901 tackle smuggling networks and hence improve global security. Tactical, because evidence that several  
902 samples seized in different locations are definitely from a common origin is very valuable information  
903 for field investigators and justice officers. Forensic laboratories are often asked to provide scientific  
904 support for an alleged link between physical evidence and a suspect or provider. In this context, the  
905 higher the number of parameters collected, the more useful the information is likely to be for  
906 forensic investigations. As illustrations of the important contribution of irm-NMR to this field, three  
907 examples are detailed below.

#### 908 **5.3.1. Pollution**

909 Just after a pollution event, a forensic enquiry asks the questions: (i) Does the sample from a polluted  
910 site really originate from the suspected source? (ii) How similar or different are the samples taken?  
911 (iii) To what extent can we predict changes between the sample taken in the field and that from the  
912 suspected source based on modelling studies of isotopic fractionation following modifying processes

913 (physical, chemical and biochemical remediation)? The inference of the source for determining the  
914 liable party is the main point that should be convincing for the judge.

915 The intramolecular  $^{13}\text{C}$  profiles of a number of molecules well-known as pollutants – MTBE (methyl  
916 *tert*-butyl ether), ETBE (ethyl *tert*-butyl ether), TAME (*tert*-amyl methyl ether), TCE (trichloroethene),  
917 n-heptane, toluene and acetone – have been determined [87]. By comparing several origins  
918 (manufacturers), it was shown that isotope profiling of the core of a molecule reveals both the raw  
919 materials and the processes used in its manufacture. An interesting case was discussed in reference  
920 [87] concerning acetone.

921

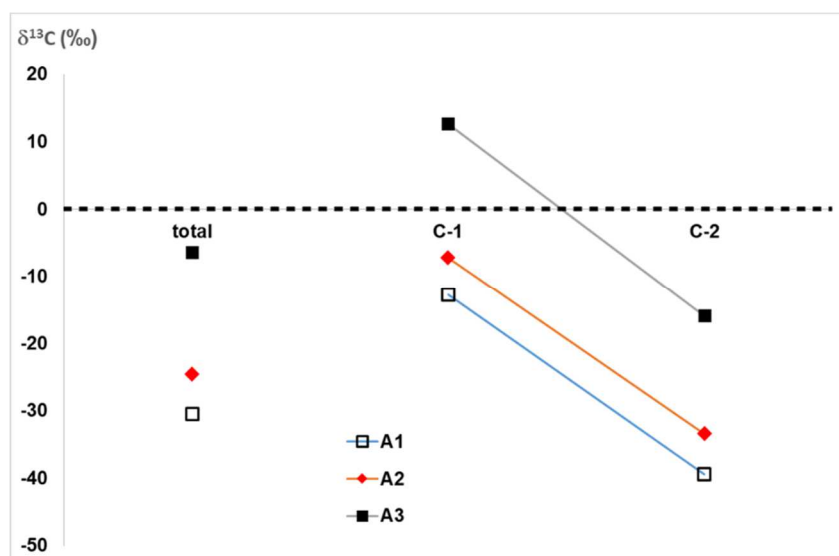
922 **Table 3:** Global  $^{13}\text{C}$  isotopic composition ( $\delta^{13}\text{C}_g$ ) and position-specific isotope composition of the carbonyl group  
923 ( $\delta^{13}\text{C}_{\text{C=O}}$ ) and the methyl moiety ( $\delta^{13}\text{C}_{\text{CH}_3}$ ) in ‰ of three acetone samples from several commercial batches.

Sample code	Provider	$\delta^{13}\text{C}_g$ (‰)	$\delta^{13}\text{C}_{\text{C=O}}$ (‰)	$\delta^{13}\text{C}_{\text{CH}_3}$ (‰)
A1	Sigma-Aldrich (Batch N° 1)	-30.6	-12.8	-39.4
A2	Sigma-Aldrich (Batch N° 2)	-24.7	-7.3	-33.4
A3	Junsei Chemical	-6.4	12.7	-16.0

924

925 **Table 3** summarizes the results for three origins of acetone. The average  $^{13}\text{C}$  content is very different  
926 for each sample, leading to dissimilar intramolecular profiles. However, the slope for each sample is  
927 the same, as illustrated in **Figure 15**. Since propylene is the raw material for the two industrial  
928 processes used by the main manufacturers (cumene process in the USA and Belgium and direct  
929 oxidation of propylene in Japan), it can be concluded that the  $^{13}\text{C}$  profile is due to the different  
930 propylene source.

931



932

933 **Figure 15:** Isotopic composition  $\delta^{13}\text{C}$  (‰) of the acetone samples (see Table 3 for origins) showing similar slopes  
 934 for the intramolecular  $^{13}\text{C}$  distribution between the samples. Total: global  $\delta^{13}\text{C}$  value measured by irm-MS. C1:  
 935 carbonyl position (C=O), C2: methyl position ( $\text{CH}_3$ ). (Adapted from [87]).

936

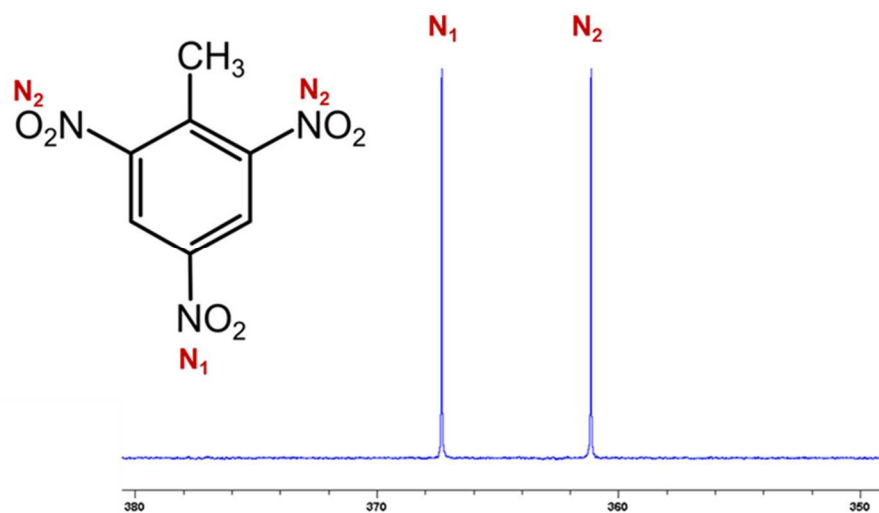
### 937 5.3.2. Explosives

938 Among all types of explosive, one category corresponds to pure compounds, including primary  
 939 explosives (initiators such as organic peroxides) and high explosives like nitro compounds such as  
 940 trinitrotoluene (TNT). The analytical strategy for explosives usually combines several technologies in  
 941 order to identify the organic and inorganic substances present both in the explosive and in the post-  
 942 explosion residues. Isotope analyses are not very common on such compounds, and even less so  
 943 those using the PSIA strategy. A recent paper employed the latest advanced methodology of irm-  
 944 NMR to construct  $^{13}\text{C}$  and  $^{15}\text{N}$  intramolecular profiles of TNT [88]. For irm- $^{13}\text{C}$  NMR, the single-pulse  
 945 method was applied, and for irm- $^{15}\text{N}$  NMR, FS-INEPT was utilized [19]. For the latter, FS-INEPT was  
 946 the only possible choice since  $^{15}\text{N}$  has very poor sensitivity (see **Table 2**) and there is no one-bond  
 947 coupling for polarization transfer in TNT. It was thus the first application of NMR spectroscopy to  $^{15}\text{N}$   
 948 PSIA (see **Figure 16** for molecular structure and  $^{15}\text{N}$  FS-INEPT spectrum).



949 As a proof of concept, 10 TNT samples collected by the French authorities were studied to compose  
950  $\delta^{13}\text{C}_i$  (from single-pulse measurement) and apparent  $\delta^{15}\text{N}_i$  (from FS-INEPT) profiles. It is worth noting  
951 here the variation scale of these isotopic compositions.

952



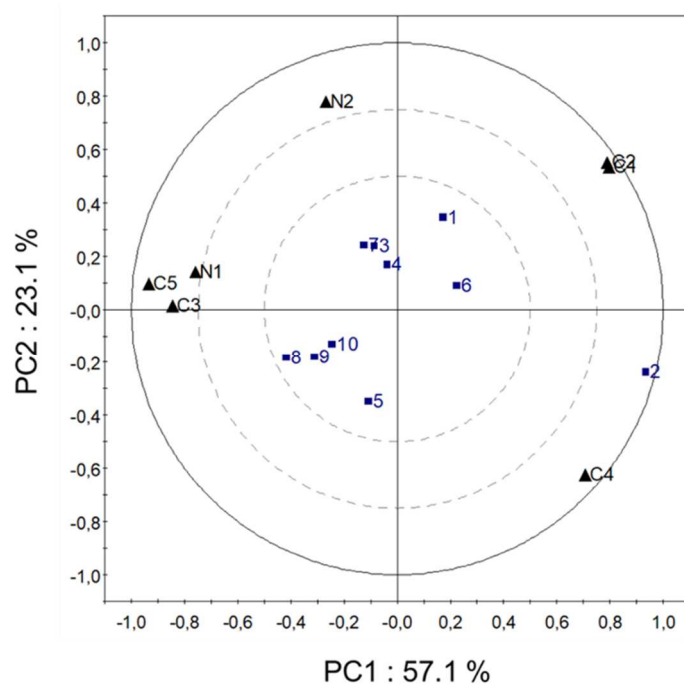
953

954 **Figure 16:** Representation of the TNT molecule with nitrogen positions numbered in decreasing  $^{15}\text{N}$  chemical  
955 shifts. Typical  $^{15}\text{N}$  NMR spectrum of a trinitrotoluene (TNT) sample obtained in about 14 h by adiabatic  
956 refocused FS-INEPT  $^{15}\text{N}$  with a signal to noise ratio of 500. (Adapted from [88]).

957

958 The use of FS-INEPT  $^{15}\text{N}$  gives only relative intensities (apparent), but the change in the  $\delta^{15}\text{N}_i$  value  
959 between samples for the same position is still on the correct scale: the difference between two given  
960 samples is due solely to the amount of  $^{15}\text{N}$  at the given position (the same isotopomer should be  
961 compared in the two samples). The change in  $\delta^{15}\text{N}_i$  can be compared to  $\delta^{15}\text{N}_g$  to evaluate their  
962 respective contribution to the discrimination of origin. For TNT, it was clear that the intramolecular  
963 isotopic compositions led to a larger number of discriminating parameters - five for  $^{13}\text{C}$  and two for  
964  $^{15}\text{N}$  - than the two collected by irm-MS.

965



966

967 **Figure 17:** Principal component analysis on TNT samples: PC1 (57.1%) vs. PC2 (23.1%) bi-plot (scores + loadings)

968 using the whole experimental variable set from  $\text{irm-}^{15}\text{N}$  NMR (FS-INEPT) and  $\text{irm-}^{13}\text{C}$  NMR (single-pulse)

969 experiments. Triangles represent the loadings (contribution of each measured parameter) used and squares

970 represent the scores (sample identification). The loadings C1 and C2 have the same position. Reprinted with

971 permission from Ref. [88]. Copyright 2020 Elsevier.

972

973 Consequently, resemblances or differences between samples are easily observed in the PCA graph

974 displaying the 10 TNT samples (**Fig. 17**). It should be noted that all the intramolecular parameters ( $^{13}\text{C}$

975 and  $^{15}\text{N}$ ) contribute to the distinction between samples, since they are close to the correlated circle

976 [88].

### 977 5.3.3. Drugs

978 In the field of illicit drugs, forensic investigations have two main objectives: (i) assigning the

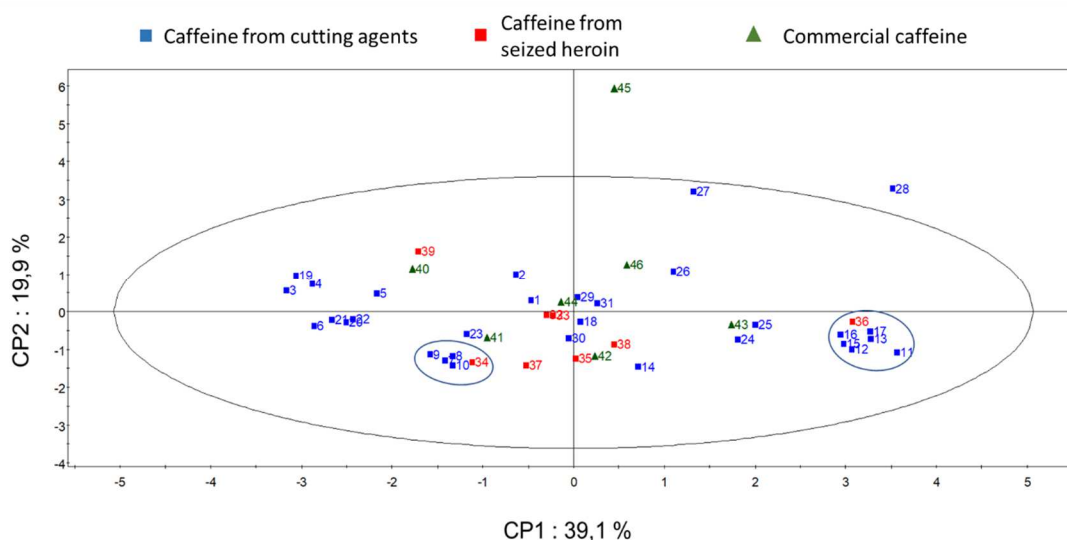
979 geographical origin of natural drugs, such as cocaine, heroin and cannabis, and (ii) determining the

980 synthetic route exploited, so as to make the link between precursors and synthetic drugs such as

981 MDMA (ecstasy) and methamphetamine. Most illicit drug samples are imported more or less pure

982 into Europe and are then gradually diluted along the trafficking chain by the addition of cutting  
 983 agents. For police investigators, knowing the active principle content is therefore an indication of the  
 984 proximity of the seized sample to its importation source. The idea of profiling a drug by focusing on  
 985 the cutting agents, rather than compounds coming from the plant or the manufacturing process, has  
 986 emerged as a completely new approach. However, regarding pharmaceuticals used as cutting agents,  
 987 very little has been done with irm-MS, except for acetaminophen and caffeine as cutting agents for  
 988 heroin.

989



990

991 **Figure 18:** Principal component analysis on caffeine samples from commercial sources, extracted from seized  
 992 cutting agents and from seized heroin: PC1 (39.1%) vs. PC2 (19.9%) score plots using the whole experimental  
 993 variable set from irm-<sup>13</sup>C NMR (FS-INEPT) experiments. The interest is to compare the caffeine from cutting  
 994 agents and from heroin samples. The two encircled zones show the similarity between seized samples: left  
 995 circle: sample 34 (from heroin) close to samples 7, 8, 9, 10 (from cutting agents from the same seizure); right  
 996 circle: sample 36 (from heroin) close to samples 11, 12, 13, 15, 16, 17 (from cutting agents from the same  
 997 seizure). (Adapted from [89]).

998

999 The application of  $^{13}\text{C}$  NMR has provided new information, as shown in a recent work [89]. A  
1000 prerequisite of the study was to analyze actual seized samples, including both cutting agents and cut  
1001 heroin. Due to the limited amount available, a specific experimental protocol was established to  
1002 purify and analyze acetaminophen and/or caffeine samples of only about 40 mg. To study such a  
1003 small mass, a combination of high magnetic field NMR spectroscopy and FS-INEPT was exploited in  
1004 order to observe all  $^{13}\text{C}$  isotopomers [18, 89]. In fact, the ratio of quaternary to other carbons in  
1005 these two molecules is not negligible. Moreover, previous analyses (from single-pulse experiments)  
1006 had shown that these quaternary carbons - three for acetaminophen and four for caffeine -  
1007 contribute significantly to the discrimination of origin, as described in Sections 5.2 and 5.4.1,  
1008 respectively [77, 83]. Once again, the isotopic compositions obtained are apparent but suitable for  
1009 statistical discrimination.

1010 Comparing the isotopic profiles of cutting agents, found pure and the same molecule that was added  
1011 in the heroin, belonging to the same seizure gives new indications about the affiliation between the  
1012 trafficking network of heroin and cutting agents. **Figure 18** confirms that the eight  $^{13}\text{C}$  isotopomers in  
1013 caffeine are similarly distributed in samples of pure cutting agents and in cut heroin samples. This is  
1014 undoubtedly new evidence that will help law authorities to dismantle criminal drug-dealing networks  
1015 in a country, independently of the origin of the drugs.

#### 1016 **5.4. Authentication**

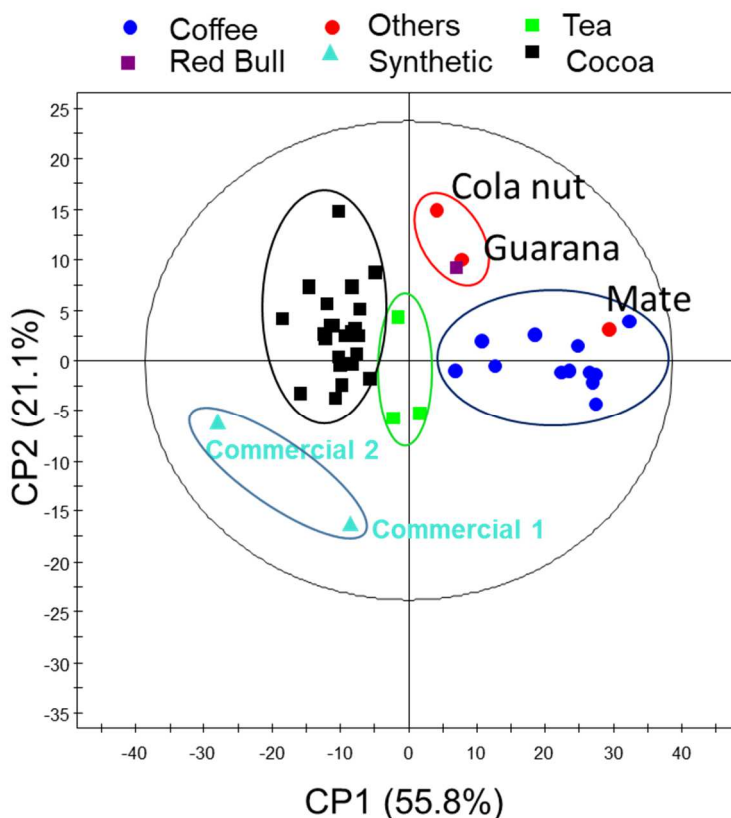
1017 In the food industry, authenticity is of particular importance. As a result, a large panel of analytical  
1018 techniques has been established to protect the health of consumers, guarantee the origin and  
1019 traceability of products, and fight against fraud, especially against the presence on the market of  
1020 EMA (Economically Motivated Adulteration). For the consumer, a falsification is a nonconformity of a  
1021 product with respect to the description on its label. The confirmation of the origin of a product is  
1022 often performed by isotope analyses because isotopic profiles are usually unique for the “molecule –  
1023 origin” couple [86]. Three examples are described in this review, to cover three aspects of

1024 authentication issues. The first is the contribution of isotopic NMR to the characterization of the  
1025 origin of caffeine. The second describes the competition between the increasing complexity of  
1026 adulteration and the response from the analytical arsenal, illustrated by vanilla flavor and its main  
1027 molecule, vanillin. The third example concerns the authentication of cholesterol for origin  
1028 investigation in food products.

### 1029 5.4.1 Caffeine

1030 Caffeine is found in relatively large amounts in coffee (0.5– 3%), tea (1–4%), mate (0.5–2%), guarana  
1031 (2–5%), cola species (1–4%), and cocoa (0.1–0.4%), while theobromine is characteristic of cocoa and  
1032 related *Theobroma* species. Caffeine is also found in energy drinks and cola-type soft drinks, that  
1033 usually contain added synthetic caffeine. The consumer expects caffeine-containing drinks to be  
1034 authentic in relation to their declared origin. For cocoa, the geographical origin concerns both the  
1035 consumers and the chocolate industry.

1036



1037

1038 **Figure 19:** Principal component analysis on caffeine samples from several sources, including theobromine from  
1039 cocoa: PC1 (55.8%) vs. PC2 (21.1%) score plots using the whole experimental variable set from  $^{13}\text{C}$  NMR  
1040 (single-pulse) experiments. (Adapted from [77]).

1041  
1042 For these two commodities, isotopic compositions contribute fully to the requirements. Within the  
1043 available methods,  $^{13}\text{C}$  NMR provides new advances in the discrimination potential.  
1044 Theobromine, due to its very low solubility in organic solvents typically used for NMR, is not an  
1045 appropriate molecular probe. A smart approach was developed by the conversion of theobromine to  
1046 caffeine by methylation [77]. As a result, caffeine is a suitable probe for studying both caffeine-  
1047 containing matrices and cocoa-based products. It appears that  $^{13}\text{C}$  profiles in caffeine are  
1048 characteristic of both the origins of caffeine-containing products (different plant origins and synthetic  
1049 caffeine) and of cocoa (geographical origins), as illustrated by **Figure 19**. It should be noted that the  
1050 application of FS-INEPT to caffeine as described in Section 5.3 led to the same patterns.

1051

#### 1052 **5.4.2. Vanillin**

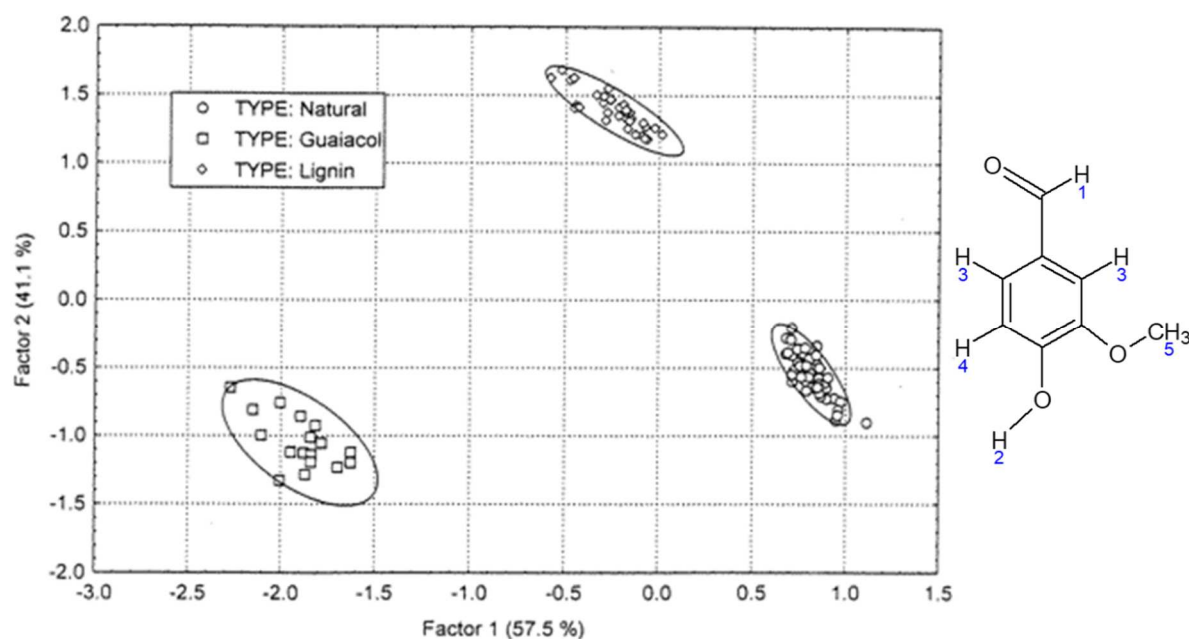
1053 A flavor can be defined as a preparation or a substance. Vanilla bean extract is defined as a flavor  
1054 preparation because it is composed of up to 200 volatile molecules of diverse chemical classes.  
1055 Vanillin is the main component (about 2% in the plant) and considered a flavor substance. Because of  
1056 its organoleptic features, vanillin is one of the flavors most used in the food and cosmetics industries,  
1057 where more than 90% of vanillin is from synthetic origins [90].

1058 An authenticity issue occurs when natural origins are claimed. In the early 1970s, the natural origin  
1059 was associated with vanilla bean extracts that could be adulterated by vanillin manufactured from  
1060 guaiacol (ex-guaiacol, synthetic) or from lignin (ex-lignin, semi-synthetic), both with an unnatural  
1061 status. At that time, the question was: is the vanillin extracted from beans?  $^{13}\text{C}$  MS was the  
1062 answer because the metabolism of vanilla is an example of CAM (Crassulacean Acid Metabolism; see

1063 Section 2.2) leading to  $\delta^{13}\text{C}_g$  of  $-20\text{‰}$  for vanillin while it is in the range from  $-29\text{‰}$  to  $-31\text{‰}$  for  
1064 unnatural origins. This is still an official method but it suffers from the easy manipulation of  $\delta^{13}\text{C}_g$  by  
1065 the addition of commercially available  $^{13}\text{C}$ -enriched vanillin [91]. An effective analytical response was  
1066 provided by  $^2\text{H}$  NMR (SNIF-NMR<sup>TM</sup> methodology) because the four resolved  $^2\text{H}$  isotopomers (the  
1067 OH position cannot be used because of its exchangeable character) were able to distinguish the  
1068 above three origins: statistically, the detection limit of adulteration was 10-15% (**Fig. 20**) [92]. This  
1069 method is recognized by official authorities [93].

1070 The last 20 years have witnessed the development of the biosynthesis of natural vanillin from several  
1071 natural precursors, as depicted in **Figure 21** [94]. The question now is: is the vanillin natural?

1072



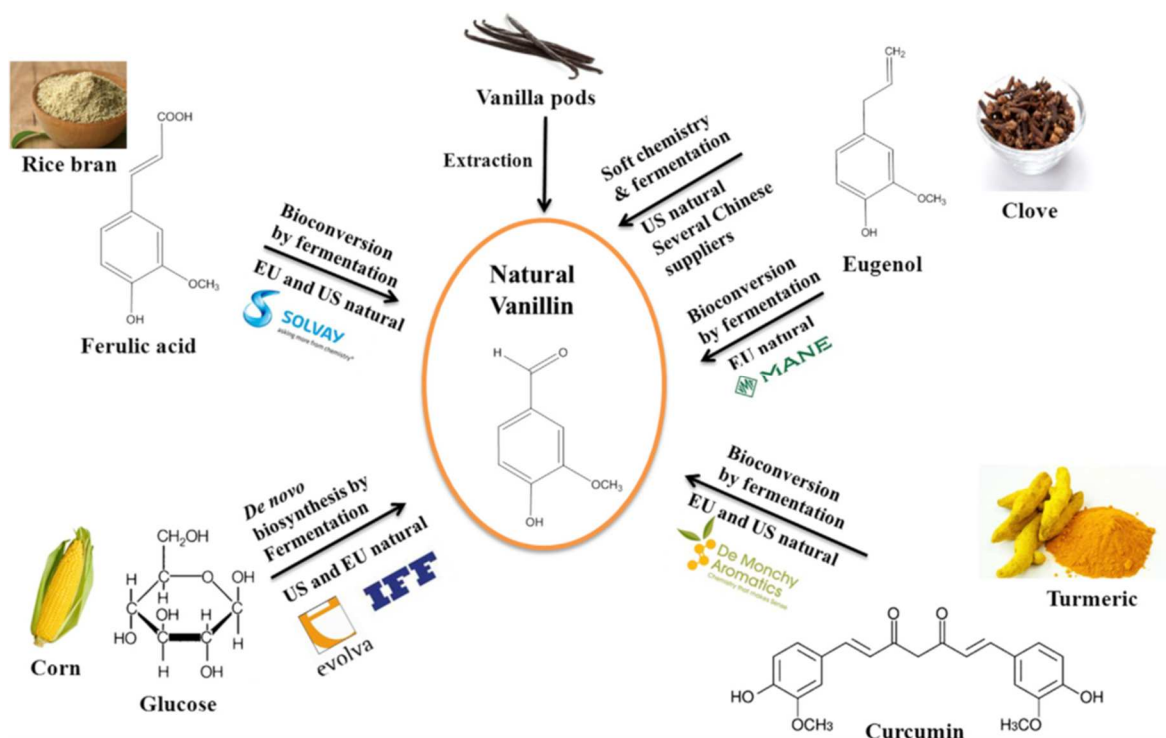
1073

1074 **Figure 20:** Representation of the reference groups of vanillin (ex-beans, ex-lignin, and ex-guaiacol) projected in  
1075 the plane of the canonical variables.  $(D/H)_1$ ,  $(D/H)_3$ ,  $(D/H)_4$ , and  $(D/H)_5$  were the initial parameters. The ellipses  
1076 drawn correspond to the 95% confidence intervals. Representation of the vanillin molecule with the  $^2\text{H}$  position  
1077 numbered in decreasing  $^2\text{H}$  chemical shifts. Reprinted with permission from Ref. [92]. Copyright 1997 ACS.

1078

1079 The answer should encompass the isotope profiles of all vanillin sources. In this context, it has been  
 1080 shown that  $^{2}\text{H}$  NMR is significantly less effective than  $^{13}\text{C}$  NMR. In fact, the eight  $^{13}\text{C}$   
 1081 isotopomers of vanillin (**Fig. 22**) enable good discrimination between different origins, including the  
 1082 geographical origin of vanilla beans [15]. Another great advantage of  $^{13}\text{C}$  NMR over  $^{2}\text{H}$  NMR is the  
 1083 smaller quantity of pure vanillin required: 250 mg *versus* 1000 mg, respectively.

1084



1085

1086 **Figure 21:** Main sources of vanillin that could be declared as natural. Reprinted with permission from Ref. [94].

1087

Copyright 2015 Elsevier.

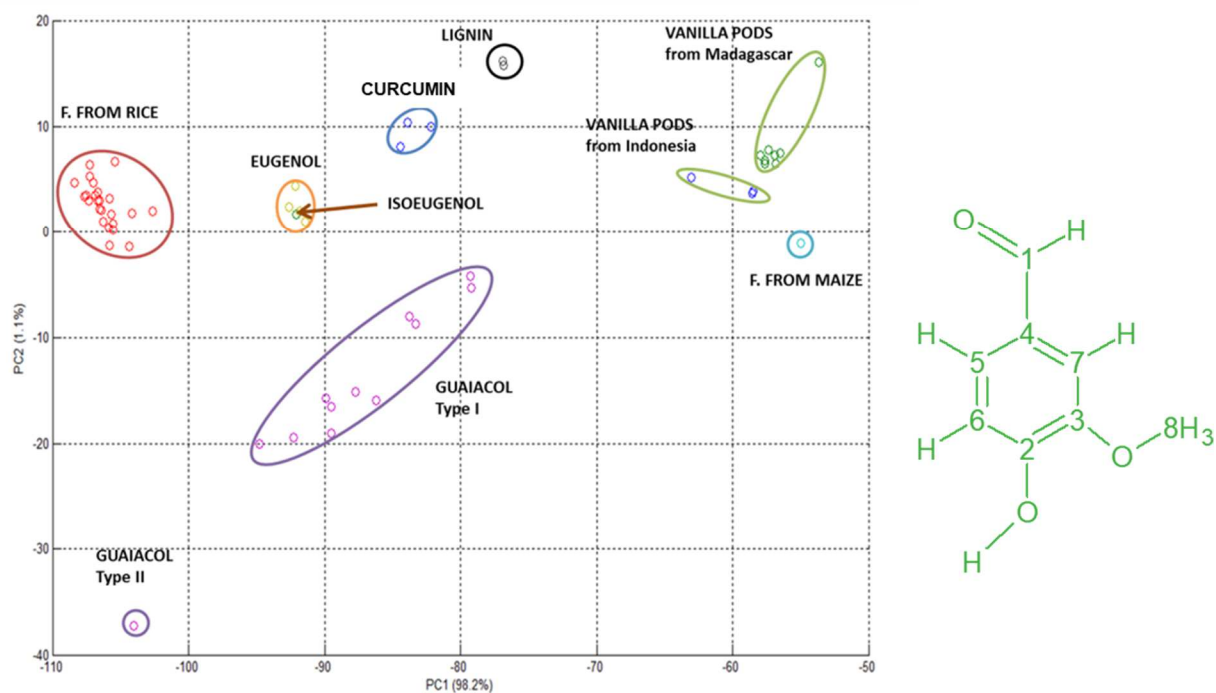
1088

1089 In [15], the authors also discuss the positions that led to the best separation of groups, the issue  
 1090 being the contribution of the quaternary carbons. In fact, the five remaining protonated isotopomers  
 1091 were responsible for the main discrimination and thus the INEPT sequence can be easily  
 1092 implemented to decrease the amount of vanillin required for a good precision (as described for other  
 1093 molecules and discussed above). It is therefore possible to study finished products, such as ice



1094 cream, yogurts or vanilla sugars, extending the level of fraud detection from industrial materials only  
1095 (extracts, flavors) to commercial end-products.

1096



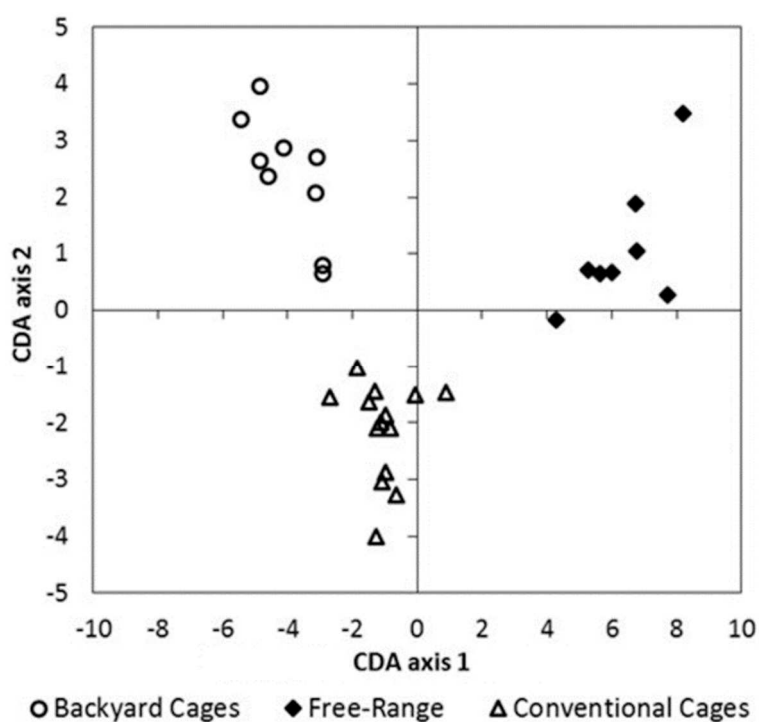
1097

1098 **Figure 22:** Two-dimensional plot of the scores obtained by PCA on the values of the <sup>13</sup>C isotopic composition for  
1099 all eight isotopomers obtained by irm-<sup>13</sup>C NMR. PC1 explains 98.2% and PC2 explains 1.1% of the total  
1100 variability over the main current sources of vanillin. Representation of the vanillin molecule with <sup>13</sup>C position  
1101 numbered in decreasing <sup>13</sup>C chemical shifts. Adapted from [15].

### 1102 5.4.3 Cholesterol

1103 Lipids are known to be quasi-universal components of food products. Their isotopic composition is  
1104 closely related to geographical origin, botanical origin and agricultural practices in the case of  
1105 products of plant origin. Cholesterol is one of the most important lipids. It is essential in cellular  
1106 organization and stability and as a building block for steroid hormones, vitamin D, oxysterols and bile  
1107 acids. However, cholesterol is also related to many health problems such as cardiovascular disease,  
1108 diabetes and high blood pressure. Furthermore, it constitutes a good model for the study of steroids.

1109 It has 27 carbon isotopomers, 22 of which are detected by carbon INEPT using one-bond couplings.  
1110 Positional carbon isotope contents were measured in order to classify egg samples according to their  
1111 origin [95]. In this work, 90 mg of cholesterol was analyzed using an optimized refocused adiabatic  
1112 INEPT. As an example of the results described in this article, **Figure 23** shows the classification of eggs  
1113 from four farming systems with eight variables: one is the global carbon content measured by irm-  
1114 MS and the others are position-specific  $^{13}\text{C}$  contents measured by NMR.  
1115



1116 **Figure 23:** Classification of egg samples according to hen farming system using eight isotopic variables obtained  
1117 from  $^{13}\text{C}$  NMR cholesterol spectra. Adapted from [95].  
1118

1119  
1120 These results are especially promising since the presented approach can be applied to cholesterol  
1121 found in other matrices like human blood. In this case, this molecule could be used as a probe to  
1122 distinguish between exogenous and endogenous sources of cholesterol. This approach could also be  
1123 applied to other steroids so the field of application can be extended to cover plant and hormone  
1124 analyses.

## 1125 **5.5. Multi-omics approach**

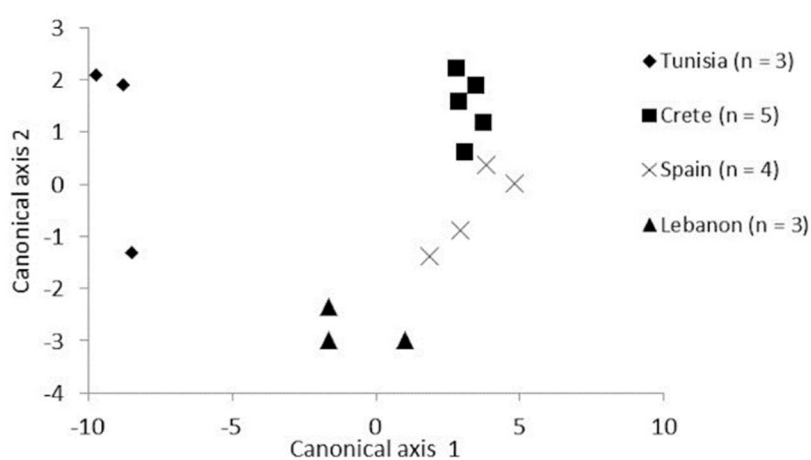
1126 The examples previously described concern pure molecules, but isotopic analysis can also be  
1127 performed on mixtures and, in these cases, a novel approach called metabisotopomics, merging  
1128 isotopic and metabolomic profiles, can efficiently be used [57]. It was first applied to the study of  
1129 triglycerides, which are quasi-universal components of food matrices and consist of complex  
1130 mixtures [96].

1131 In the carbon spectrum of such a mixture, the peak areas depend on the isotope abundances as well  
1132 as concentrations. So, to determine the isotope content, it is essential to know the concentration  
1133 with high precision. In triglycerides, the composition in fatty acids cannot be known with a precision  
1134 as high as a few permil. Therefore, most of the peaks observed in the  $^{13}\text{C}$  NMR spectrum can only be  
1135 used as compositional profile elements, and not for measurement of the intramolecular isotopic  
1136 distribution. However, the NMR signals related to the carbons of the glycerol moiety, the first part of  
1137 the fatty acids (C2 and C3), and the terminal methyl groups, are always present, and are common to  
1138 all triglyceride molecules. This enables them to be used for isotopic purposes. Isotopic variables can  
1139 also be obtained from the ratios between two peaks of the same compound. When the SNR is high  
1140 enough, these two profiles, isotopic and metabolomic, can be obtained from the same carbon  
1141 spectrum.

1142 This method was applied to classify olive oils according to their geographical origin [96]. Only two  
1143 ratios are needed, one from the isotopic profile and one from the metabolic profile. The former is  
1144 the relative isotope abundance of the glycerol carbons and the latter is the relative amount of  
1145 linoleic acid at the *sn1* or *sn3* position, with respect to that at the *sn2* position. Moreover, full  
1146 deconvolution of the INEPT spectrum of olive oil provides up to 80 variables (isotopic or  
1147 metabolomic) which can be used to obtain the complete profile of triglyceride mixtures, *i.e.* oil  
1148 composition, positional distribution of fatty acids on the glycerol backbone, and some position-

1149 specific  $^{13}\text{C}$  content [96]. The same approach can be used to authenticate triacylglycerols of animal  
1150 origin [95].

1151 This strategy can be extended to 2D NMR, which is an attractive alternative to 1D in order to avoid or  
1152 limit the overlap of peaks observed in complex mixtures. In order to decrease the experimental time  
1153 of a 2D acquisition ( $^1\text{H}$ - $^{13}\text{C}$  HSQC) a strategy was developed by Merchak *et al.* [50] which consists of  
1154 choosing, along the indirect dimension, a spectral width smaller than the  $^{13}\text{C}$  chemical shift  
1155 dispersion.



1156  
1157 **Fig. 24:** Classification of vegetable oils using variables from their corresponding HSQC spectra according to their  
1158 geographical origin. Adapted from [50].

1159  
1160 The peaks violating the Nyquist condition are then aliased and the spectral range to be sampled in  $F_1$   
1161 is therefore smaller, reducing the number of  $t_1$  increments required to achieve a given  $F_1$  resolution.  
1162 Additionally, non-uniform sampling is used to halve the number of increments in the  $F_1$  dimension  
1163 for the same experiment duration, even if it could degrade the reliability of quantitation. With this  
1164 strategy, the experimental time was reduced to 22 minutes.

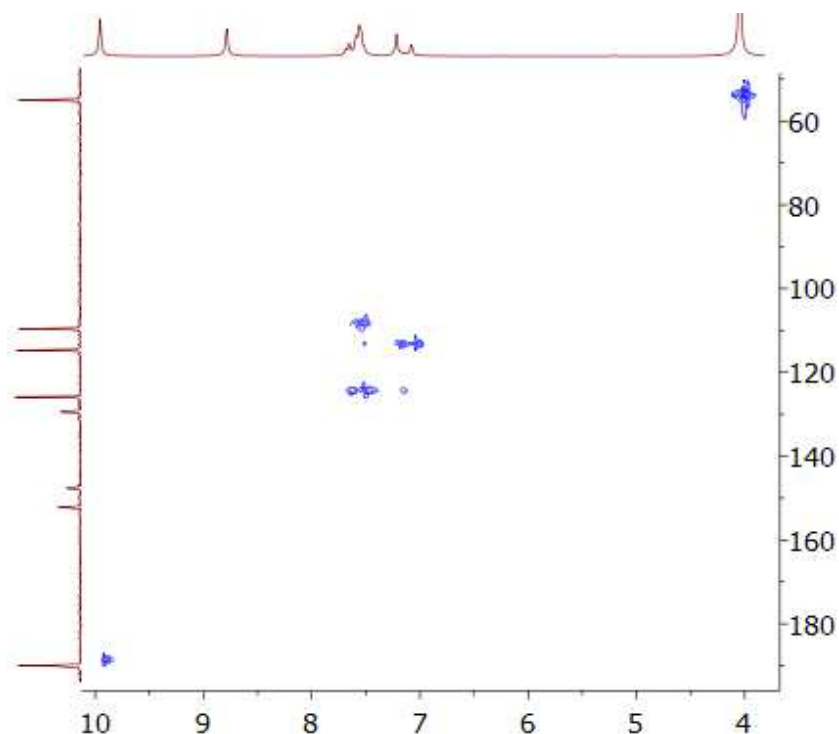
1165 **Figure 24** shows that such a strategy enables edible oils to be classified according to their  
1166 geographical or botanical origin [50].

1167



## 1169 **6. Concluding remarks and perspectives**

1170 For organic matter, the abundance of  $^2\text{H}$ ,  $^{13}\text{C}$ ,  $^{15}\text{N}$ ,  $^{18}\text{O}$  or  $^{34}\text{S}$  isotopologues -relative to the  
1171 corresponding lighter species- are routinely determined by irm-MS with a high level of automation.  
1172 This on-line technique leads to high precision: standard deviation lower than 0.3‰ (on the isotopic  
1173 composition  $\delta$ -scale) on a small amount of material (of the order of mg). However, the  
1174 intramolecular isotopic distribution is not available since only the mean heavy isotope content  
1175 (global composition) is accessible. However, since a given molecule is constituted of a mixture of  
1176 isomers (isotopomers), it needs to be taken into account that these could behave independently and  
1177 differently. Position-specific isotope analysis (PSIA) reveals the isotopomer distribution within a  
1178 molecule, and NMR spectroscopy is a well-adapted tool for separating the respective signals and  
1179 quantifying them. Historically,  $^2\text{H}$  NMR was the first approach able to show the interest of PSIA.  
1180 Further developments have led to the use of irm- $^{13}\text{C}$  NMR and, more recently, irm- $^{15}\text{N}$  NMR. Beside  
1181 the NMR core of this review, in which all parameters are described to establish the optimum  
1182 protocol, examples of applications of irm-NMR illustrate the information retrieved from typical actual  
1183 cases and how the analytical protocol should be adapted according to the questions to be addressed.  
1184 While a huge amount of information has already been collected, further improvements are on-going.  
1185 The high precision required imposes significant constraints on NMR experiments. Multi-pulse  
1186 sequences can be used to overcome these drawbacks and thereby reduce the minimum amount of  
1187 material needed for irm- $^{13}\text{C}$  NMR, or to explore other nuclei, as has been done with  $^{15}\text{N}$ .  
1188 It is now expected that new challenges will be tackled during the next decade, since preliminary work  
1189 is converging toward encouraging prospects. Recent advances in 2D NMR promise further  
1190 improvements in sensitivity, which will allow  $^{13}\text{C}$  measurement with only a few mg, or the use of  
1191 benchtop NMR spectrometers. As an illustration, **Figure 25** shows the 2D spectrum of vanillin  
1192 obtained on a low-field spectrometer, indicating that in some conditions good precision could be  
1193 reached for irm- $^{13}\text{C}$  NMR on affordable NMR spectrometers for most industrial fields.



1194

1195 **Figure 25:** HSQC  $^1\text{H}$ - $^{13}\text{C}$  spectrum of vanillin (215 mg in 0.75 mL of acetone- $d_6$ ) obtained on a low-field (80 MHz)

1196

Spinsolve spectrometer. Reprinted with permission from Magritek.

1197

1198 PSIA  $^{17}\text{O}$  is not yet described in the literature. In the context of the MIF (Mass Independent

1199 Fractionation) theory, it could be rewarding to compare the  $^{18}\text{O}$  versus  $^{17}\text{O}$  fractionation in organic

1200 matter as it occurs in gases such as  $\text{O}_3$ ,  $\text{CO}_2$ ,  $\text{N}_2\text{O}$ , etc. [97]. Beside the interest in  $^{17}\text{O}$ , the bi-labeled

1201 clumped isotopologue  $^{13}\text{C}$ - $^{13}\text{C}$  at natural abundance could provide novel information [2].

1202 After reading this review, we hope that new users will join the isotopomics community and

1203 contribute to extending such applications, which have already given notable results.

1204

1205

1206 **Acknowledgements**

1207 The authors thank Carol Wigglesworth and Richard Robins for fruitful suggestions and linguistic  
1208 correction. This review was supported by the National Aeronautics and Space Administration through  
1209 the NASA Astrobiology Institute under Cooperative Agreement No. 80NSSC18M0094 issued through  
1210 the Science Mission Directorate.

1211



## 1212 References

- 1213 1- H.-L. Schmidt, R. J. Robins, R. A. Werner. Multi-factorial in vivo stable isotope fractionation: causes,  
1214 correlations, consequences and applications. *Isotopes Environ. Health Stud.* 51 (2015) 155–199.  
1215 <http://dx.doi.org/10.1080/10256016.2015.1014355>
- 1216 2- J. M. Eiler. The Isotopic Anatomies of Molecules and Minerals. *Annu. Rev. Earth Planet. Sci.* 41  
1217 (2013) 411-441. <https://doi.org/10.1146/annurev-earth-042711-105348>
- 1218 3- Z. Muccio, G. P. Jackson. Isotope ratio mass spectrometry, *Analyst.* 134 (2009) 213–222.  
1219 <https://doi:10.1039/B808232D>.
- 1220 4- I. Tea, G. Tcherkez. Natural Isotope Abundance in Metabolites: Techniques and kinetic isotope  
1221 effect measurement in plant, animal, and human tissues. In: Harris M. E. and Anderson V. E., Editors.  
1222 *Methods in Enzymology* (Vol. 596). Cambridge. Academic Press. 2017, pp. 113-147. [https://](https://dx.doi.org/10.1016/bs.mie.2017.07.020)  
1223 [dx.doi.org/10.1016/bs.mie.2017.07.020](https://dx.doi.org/10.1016/bs.mie.2017.07.020)
- 1224 5- R. Dias, K. Freeman, S. Franks. Gas chromatography–pyrolysis–isotope ratio mass spectrometry: a  
1225 new method for investigating intramolecular isotopic variation in low molecular weight organic acids.  
1226 *Org. Geochem.* 33 (2002) 161-168. [https://doi.org/10.1016/S0146-6380\(01\)00141-3](https://doi.org/10.1016/S0146-6380(01)00141-3)
- 1227 6- C. Gauchotte-Lindsay, S. Turnbull. On-line high-precision carbon position-specific stable isotope  
1228 analysis: A review. *TrAC Trends in Anal. Chem.* 76 (2016) 115-125. [https://doi.org/10.1016/](https://doi.org/10.1016/j.trac.2015.07.010)  
1229 [j.trac.2015.07.010](https://doi.org/10.1016/j.trac.2015.07.010)
- 1230 7- G. J. Martin, M. L. Martin. Deuterium labelling at the natural abundance level as studied by high  
1231 field quantitative  $^2\text{H}$  NMR. *Tetrahedron Lett.* 22 (1981) 3525-3528. [https://doi.org/10.1016/S0040-](https://doi.org/10.1016/S0040-4039(01)81948-1)  
1232 [4039\(01\)81948-1](https://doi.org/10.1016/S0040-4039(01)81948-1)
- 1233 8- E. Jamin, F. Thomas. SNIF-NMR Applications in an Economic Context: Fraud Detection in Food  
1234 Products, in: *Mod. Magn. Reson.*, Springer, Cham, 2017: pp. 1–12. [https://doi:10.1007/978-3-319-](https://doi:10.1007/978-3-319-28275-6_103-1)  
1235 [28275-6\\_103-1](https://doi:10.1007/978-3-319-28275-6_103-1)
- 1236 9- P. Lesot, C. Aroulanda, P. Berdagué, A. Meddour, D. Merlet, J. Farjon, N. Giraud, O. Lafon.  
1237 Multinuclear NMR in polypeptide liquid crystals: Three fertile decades of methodological  
1238 developments and analytical challenges. *Prog. Nucl. Magn. Reson. Spectrosc.* 116 (2020) 85-154.  
1239 <https://doi.org/10.1016/j.pnmrs.2019.10.001>
- 1240 10- J. M. Hayes. Fractionation of the isotopes of carbon and hydrogen in biosynthetic processes. *Rev.*  
1241 *Mineral Geochem.* 43 (2001) 225–277. <https://doi.org/10.2138/gsrmg.43.1.225>
- 1242 11- V. Caer, M. Trierweiler, G. J. Martin, M. L. Martin. Determination of site-specific carbon isotope  
1243 ratios at natural abundance by carbon-13 nuclear magnetic resonance spectroscopy. *Anal. Chem.* 63  
1244 (1991) 2306-2313. <https://doi.org/10.1021/ac00020a021>
- 1245 12- B.-L. Zhang, S. Buddrus, M. Trierweiler, G. J. Martin. Characterization of Glycerol from Different  
1246 Origins by  $^2\text{H}$ - and  $^{13}\text{C}$ -NMR Studies of Site-Specific Natural Isotope Fractionation. *J. Agric. Food*  
1247 *Chem.* 46 (1998) 1374–1380. <https://doi.org/10.1021/jf970794+>
- 1248 13- E. Caytan, G. Remaud, E. Tenailleau, S. Akoka. Precise and accurate quantitative  $^{13}\text{C}$  NMR with  
1249 reduced experimental time. *Talanta* 71 (2007) 1016–1021. [https://doi.org/10.1016/j.talanta.](https://doi.org/10.1016/j.talanta.2006.05.075)  
1250 [2006.05.075](https://doi.org/10.1016/j.talanta.2006.05.075)

- 1251 14- E. Caytan, E. P. Botosoa, V. Silvestre, R. J. Robins, S. Akoka, G. S. Remaud. Accurate Quantitative  
1252 <sup>13</sup>C NMR Spectroscopy: Repeatability over Time of Site-Specific <sup>13</sup>C Isotope Ratio Determination. *Anal.*  
1253 *Chem.* 79 (2007) 8266–8269. <https://doi.org/10.1021/ac070826k>.
- 1254 15- S. Guyader, F. Thomas, E. Jamin, M. Grand, S. Akoka, V. Silvestre, G. S. Remaud. Combination of  
1255 <sup>13</sup>C and <sup>2</sup>H SNIF-NMR isotopic fingerprints of vanillin to control its precursors. *Flavour Fragr. J.* 34  
1256 (2019) 133–144. <https://doi.org/10.1002/ffj.3486>
- 1257 16- C. Thibaudeau, G. S. Remaud, V. Silvestre, S. Akoka. Performance Evaluation of Quantitative  
1258 Adiabatic <sup>13</sup>C NMR Pulse Sequences for Site-Specific Isotopic Measurements. *Anal. Chem.* 82 (2010)  
1259 5582–5590. <https://doi.org/10.1021/ac100478h>.
- 1260 17- G. Tcherkez, J. Ghashghaie, H. Griffiths. Methods for improving the visualization and  
1261 deconvolution of isotopic signals. *Plant Cell Environ.* 30 (2007) 887–891. <https://dx.doi.org/10.1111/j.1365-3040.2007.01687.x>
- 1263 18- V. Joubert, V. Silvestre, M. Grand, D. Loquet, V. Ladroue, F. Besacier, S. Akoka, G. S. Remaud. Full  
1264 spectrum isotopic <sup>13</sup>C NMR using polarization transfer for position-specific isotope analysis. *Anal.*  
1265 *Chem.* 90 (2018) 8692–8699. <https://pubs.acs.org/doi/10.1021/acs.analchem.8b02139>.
- 1266 19- V. Joubert, V. Silvestre, M. Lelièvre, V. Ladroue, F. Besacier, S. Akoka, G. S. Remaud. Position-  
1267 specific <sup>15</sup>N isotope analysis in organic molecules: A high-precision <sup>15</sup>N NMR method to determine the  
1268 intramolecular <sup>15</sup>N isotope composition and fractionation at natural abundance. *Magn. Reson. Chem.*  
1269 57 (2019) 1136–1142. DOI: 10.1002/mrc.4903
- 1270 20- T. B. Coplen, Guidelines and recommended terms for expression of stable-isotope-ratio and gas-  
1271 ratio measurement results. *Rapid Commun. Mass Spectrom.* 25 (2011) 2538–2560. <https://doi.org/10.1002/rcm.5129>
- 1273 21- T. Jézéquel, V. Joubert, P. Giraudeau, G. S. Remaud, S. Akoka. The new face of isotopic NMR at  
1274 natural abundance. *Magn. Reson. Chem.* 55 (2017) 77–90. <https://doi.org/10.1002/mrc.4548>
- 1275 22- G. S. Remaud, S. Akoka. Review of flavors authentication by position-specific isotope analysis by  
1276 nuclear magnetic resonance spectrometry: the example of vanillin. *Flavour Fragr. J.* 32 (2017) 77–84.  
1277 <https://doi.org/10.1002/ffj.3366>
- 1278 23- I. D. Clark (1998) Isotope fractionation. In: *Geochemistry. Encyclopedia of Earth Science.* Springer,  
1279 Dordrecht. <https://doi.org/10.1007/1-4020-4496-8>
- 1280 24- G. D. Farquhar, J. R. Ehleringer, K. T. Hubick. Carbon Isotope Discrimination and Photosynthesis.  
1281 *Annu. Rev. Plant Physiol. Plant Mol. Biol.* 40 (1989) 503–537. [https://doi.org/10.1146/annurev.pp.40.](https://doi.org/10.1146/annurev.pp.40.060189.002443)  
1282 060189.002443
- 1283 25- T. B. Hofstetter, M. Berg. Assessing transformation processes of organic contaminants by  
1284 compound-specific stable isotope analysis. *Trends Anal. Chem.* 30 (2011) 618–627. <https://doi.org/10.1016/j.trac.2010.10.012>.
- 1286 26- M. Thullner, F. Centler, H.-H. Richnow, A. Fischer. Quantification of organic pollutant degradation  
1287 in contaminated aquifers using compound specific stable isotope analysis – Review of recent  
1288 developments. *Org. Geochem.* 42 (2012) 1440–1460. [https://doi.org/10.1016/j.orggeochem.](https://doi.org/10.1016/j.orggeochem.2011.10.011)  
1289 2011.10.011
- 1290 27- D. Bouchard, D. Hunkeler, P. Höhener. Carbon isotope fractionation during aerobic  
1291 biodegradation of n-alkanes and aromatic compounds in unsaturated sand. *Org. Geochem.* 39 (2008)  
1292 23–33. <https://doi.org/10.1016/j.orggeochem.2007.10.002>.

- 1293 28- P. H. Abelson, T. C. Hoering. Carbon isotope fractionation in formation of amino acids by  
1294 photosynthetic organisms. *Proc. Natl. Acad. Sci. U.S.A.* 47 (1961) 623-632. [https://doi.org/10.1073/](https://doi.org/10.1073/pnas.47.5.623)  
1295 [pnas.47.5.623](https://doi.org/10.1073/pnas.47.5.623).
- 1296 29- K. Yamada, M. Tanaka, F. Nakagawa, N. Yoshida. On-line measurement of intramolecular carbon  
1297 isotope distribution of acetic acid by continuous-flow isotope ratio mass spectrometry. *Rapid*  
1298 *Commun. Mass Spectrom.* 16 (2002) 1059–1064. <https://doi.org/10.1002/rcm.678>.
- 1299 30- J. M. Eiler, B. Bergquist, I. Bourg, P. Cartigny, J. Farquhar, A. Gagnon, W. Guo, I. Halevy, A.  
1300 Hofmann, T. E. Larson, N. Levin, E. A. Schauble, D. Stolper. *Frontiers of stable isotope geoscience.*  
1301 *Chem. Geol.* 372 (2014) 119–143. <https://doi.org/10.1016/j.chemgeo.2014.02.006>.
- 1302 31- G. S. Remaud, P. Giraudeau, P. Lesot, S. Akoka. Isotope Ratio Monitoring by NMR. Part 1: Recent  
1303 Advances. In: Webb G. (eds) *Modern Magnetic Resonance*. Springer, Cham, 2017.
- 1304 32- A. Menditto, M. Patriarca, B. Magnusson. Understanding the meaning of accuracy, trueness and  
1305 precision. *Accred. Qual. Assur.* 12 (2007) 45–47. <https://doi.org/10.1007/s00769-006-0191-z>
- 1306 33- JCGM: Joint Committee for Guides in Metrology, International vocabulary of metrology – Basic  
1307 and general concepts and associated terms (VIM). *JCGM 200:2012*.
- 1308 34- E. Prenesti, F. Gosmaro. Trueness, precision and accuracy: a critical overview of the concepts as  
1309 well as proposals for revision. *Accred. Qual. Assur.* 20 (2015) 33–40. [https://doi.org/10.1007/s00769-](https://doi.org/10.1007/s00769-014-1093-0)  
1310 [014-1093-0](https://doi.org/10.1007/s00769-014-1093-0)
- 1311 35- P. Giraudeau, I. Tea, G. Remaud, S. Akoka. Reference and normalization methods: Essential tools  
1312 for the intercomparison of NMR spectra. *J. Pharm. Biomed. Anal.* 93 (2014) 3–16.  
1313 <http://dx.doi.org/10.1016/j.jpba.2013.07.020>
- 1314 36- R. R. Ernst, G. Bodenhausen, A. Wokaun. *Principles of Nuclear Magnetic Resonance in One and*  
1315 *Two Dimensions*, Oxford University Press, New York, 1991.
- 1316 37- D. J. Cookson, B. E. Smith. Optimal conditions for obtaining quantitative <sup>13</sup>C NMR Data. *J. Magn.*  
1317 *Reson.* 57 (1984) 355-368. [https://doi.org/10.1016/0022-2364\(84\)90253-1](https://doi.org/10.1016/0022-2364(84)90253-1).
- 1318 38- S. Gillet, J.-J. Delpuech. Optimum conditions for nondestructive quantitative analysis by carbon-  
1319 13 NMR. *J. Magn. Reson.* 38 (1980) 433-445. [https://doi.org/10.1016/0022-2364\(80\)90325-X](https://doi.org/10.1016/0022-2364(80)90325-X)
- 1320 39- D. J. Cookson, B. E. Smith. Optimal experimental parameters for quantitative pulse Fourier  
1321 transform proton nuclear magnetic resonance spectrometry. *Anal. Chem.* 54 (1982) 2591–3.  
1322 <https://doi.org/10.1021/ac00251a042>
- 1323 40- E. Tenaillon, G. S. Remaud, S. Akoka. Quantification of the <sup>1</sup>H-decoupling effects on the accuracy  
1324 of <sup>13</sup>C-NMR measurements. *Instrum. Sci. Technol.* 33 (2005) 391-399. [https://doi.org/10.1081/CI-](https://doi.org/10.1081/CI-200063700)  
1325 [200063700](https://doi.org/10.1081/CI-200063700).
- 1326 41- E. Tenaillon, S. Akoka. Adiabatic <sup>1</sup>H decoupling scheme for very accurate intensity  
1327 measurements in <sup>13</sup>C-NMR. *J. Magn. Reson.* 185 (2007) 50-58. [https://doi.org/10.1016/j.jmr.](https://doi.org/10.1016/j.jmr.2006.11.007)  
1328 [2006.11.007](https://doi.org/10.1016/j.jmr.2006.11.007)
- 1329 42- F. Schilling, L. R. Warner, N. I. Gershenson, T. E. Skinner, M. Sattler, S. J. Glaser. Next-generation  
1330 heteronuclear decoupling for high-field biomolecular NMR spectroscopy. *Angew. Chem. Int. Ed.* 53  
1331 (2014) 4475-4479. <https://doi.org/10.1002/anie.201400178>
- 1332 43- A. Tannus, M. Garwood. Improved performance of frequency-swept pulses using offset-  
1333 independent adiabaticity. *J. Magn. Reson. A* 120 (1996) 133–137. <https://doi.org/10.1006/jmra.1996>  
1334 [.0110](https://doi.org/10.1006/jmra.1996).

- 1335 44- N. Karabulut, E. Baguet, M. Trierweiler, S. Akoka. Improvement in quantitative accuracy of  $^{13}\text{C}$   
1336 DEPT integrals by parameter-optimization. *Anal. Lett.* 35 (2002) 2549–2563. [https://doi.org/10.1081/  
1337 AL-120016544](https://doi.org/10.1081/AL-120016544)
- 1338 45- T. Saito, S. Nakaie, M. Kinoshita, T. Ihara, S. Kinugasa, A. Nomura, T. Maeda. Practical guide for  
1339 accurate quantitative solution state NMR analysis. *Metrologica* 41 (2004) 213–218. [https://doi.org/  
1340 10.1088/0026-1394/41/3/015](https://doi.org/10.1088/0026-1394/41/3/015)
- 1341 46- U. Holzgrabe. Quantitative NMR spectroscopy in pharmaceutical applications. *Prog. Nucl. Magn.*  
1342 *Reson. Spectrosc.* 57 (2010) 229–240. <https://doi.org/10.1016/j.pnmrs.2010.05.001>.
- 1343 47- S. K. Bharti, R. Roy. Quantitative  $^1\text{H}$  NMR spectroscopy. *TrAC Trends Anal. Chem.* 35 (2012) 5–26.  
1344 <https://doi.org/10.1016/j.trac.2012.02.007>.
- 1345 48- R. J. Robins, G. S. Remaud, S. Akoka. Isotope Ratio Monitoring  $^{13}\text{C}$  Nuclear Magnetic Resonance  
1346 Spectrometry for the Analysis of Position-Specific Isotope Ratios. In: Harris M. E. and Anderson V. E.,  
1347 Editors. *Methods in Enzymology* (Vol. 596). Cambridge. Academic Press, 2017.
- 1348 49- U. Bussy, C. Thibaudeau, F. Thomas, J.-R. Desmurs, E. Jamin, G. S. Remaud, V. Silvestre, S. Akoka.  
1349 Isotopic finger-printing of active pharmaceutical ingredients by  $^{13}\text{C}$  NMR and polarization transfer  
1350 techniques as a tool to fight against counterfeiting. *Talanta* 85 (2011) 1909–1914. [https://doi.org/  
1351 10.1016/j.talanta.2011.07.022](https://doi.org/10.1016/j.talanta.2011.07.022).
- 1352 50- N. Merchak, V. Silvestre, L. Rouger, P. Giraudeau, T. Rizk, J. Bejjani, S. Akoka. Precise and rapid  
1353 isotopic analysis by  $^1\text{H}$ - $^{13}\text{C}$  2D NMR: Application to triacylglycerol matrices. *Talanta* 156–157 (2016)  
1354 239–244. <https://doi.org/10.1016/j.talanta.2016.05.031>.
- 1355 51- A. Chaintreau, W. Fieber, H. Sommer, A. Gilbert, K. Yamada, N. Yoshida, A. Pagelot, D. Moskau, A.  
1356 Moreno, J. Schleucher, F. Reiniero, M. Holland, C. Guillou, V. Silvestre, S. Akoka, G. S. Remaud. Site-  
1357 specific  $^{13}\text{C}$  content by quantitative isotopic  $^{13}\text{C}$  Nuclear Magnetic Resonance Spectrometry: a pilot  
1358 inter-laboratory study. *Anal. Chim. Acta* 788 (2013) 108–113. [https://doi.org/10.1016/j.aca.2013.  
1359 06.004](https://doi.org/10.1016/j.aca.2013.06.004).
- 1360 52- E. Martineau, S. Akoka, R. Boisseau, B. Delanoue, P. Giraudeau. Fast Quantitative  $^1\text{H}$ - $^{13}\text{C}$  Two-  
1361 Dimensional NMR with Very High Precision. *Anal. Chem.* 85 (2013) 4777–4783. [https://doi.org/  
1362 10.1021/ac4005309](https://doi.org/10.1021/ac4005309).
- 1363 53- T. Schoenberger, S. Menges, M.A. Bernstein. Improving the performance of high-precision qNMR  
1364 measurements by a double integration procedure in practical cases. *Anal. Chem.* 88 (2016) 3836–  
1365 3843. <https://doi.org/10.1021/acs.analchem.5b04911>
- 1366 54- R. Laatikainen, M. Tiainen, S.-P. Korhonen, M. Niemitz. Computerized Analysis of High-resolution  
1367 Solution-state Spectra. *Encyclopedia of Magnetic Resonance* on line, John Wiley & Sons; 2011.  
1368 <https://doi.org/10.1002/9780470034590.emrstm1226>.
- 1369 55- S. Sokolenko, T. Jezequel, G. Hajjar, J. Farjon, S. Akoka, P. Giraudeau. Robust 1D NMR lineshape  
1370 fitting using real and imaginary data in the frequency domain. *J. Magn. Reson.* 298 (2019) 91–100.  
1371 <https://doi.org/10.1016/j.jmr.2018.11.004>.
- 1372 56- E. Tenailleau, P. Lancelin, R. J. Robins, S. Akoka, Authentication of the origin of vanillin using  
1373 quantitative natural abundance  $^{13}\text{C}$  NMR. *J. Agric. Food Chem.* 52 (2004) 7782–7787. [https://doi.org/  
1374 10.1021/jf048847s](https://doi.org/10.1021/jf048847s).
- 1375 57- N. Merchak, J. Bejjani, T. Rizk, V. Silvestre, G. S. Remaud, S. Akoka.  $^{13}\text{C}$  isotopomics of  
1376 triacylglycerols using NMR with polarization transfer techniques. *Anal. Methods* 7 (2015) 4889–4891.  
1377 <https://doi.org/10.1039/C5AY01250C>.

- 1378 58- M. L. Martin, S. Akoka, G. J. Martin, SNIF-NMR – Part 1: Principles. In: Webb G. A., editor. Modern  
1379 magnetic resonance. Dordrecht: Springer; 2006.
- 1380 59- C. Fauhl, R. Z. Wittkowski. On line H-1-NMR to facilitate tube preparation in SNIF-NMR analysis. Z.  
1381 Lebensm. Unters. Forsch. 203 (1996) 541–5. <https://doi.org/10.1007/BF01193160>.
- 1382 60- T. Jézéquel, V. Silvestre, K. Dinis, P. Giraudeau, S. Akoka. Optimized slice-selective  $^1\text{H}$  NMR  
1383 experiments combined with highly accurate quantitative  $^{13}\text{C}$  NMR using an internal reference  
1384 method. J. Magn. Res. 289 (2018) 18-25. <https://doi.org/10.1016/j.jmr.2018.02.002>
- 1385 61- K. Bayle, M. Grand, A. Chaintreau, R. J. Robins, W. Fieber, H. Sommer, S. Akoka, G. S. Remaud.  
1386 Internal referencing for  $^{13}\text{C}$  position-specific isotope analysis measured by NMR spectrometry. Anal.  
1387 Chem. 87 (2015) 7550-4. <https://doi.org/10.1021/acs.analchem.5b02094>.
- 1388 62- B.-L. Zhang, M. Trierweiler, C. Jouitteau, G. J. Martin. Consistency of NMR and Mass Spectrometry  
1389 determinations of natural abundance site-specific carbon isotope ratios. The case of Glycerol. Anal.  
1390 Chem. 71 (1999) 2301-2306. <https://doi.org/10.1021/ac9812375>.
- 1391 63- A. Gilbert, R. Hattori, V. Silvestre, N. Wasano, S. Akoka, S. Hirano, K. Yamada, N. Yoshida, G. S.  
1392 Remaud. Comparison of IRMS and NMR spectrometry for the determination of intramolecular  $^{13}\text{C}$   
1393 isotope composition: Application to ethanol. Talanta 99 (2012) 1035–1039. [http://dx.doi.org/](http://dx.doi.org/10.1016/j.talanta.2012.05.023)  
1394 [10.1016/j.talanta.2012.05.023](http://dx.doi.org/10.1016/j.talanta.2012.05.023)
- 1395 64- K. Bayle, A. Gilbert, M. Julien, K. Yamada, V. Silvestre, R. J. Robins, S. Akoka, N. Yoshida, G. S.  
1396 Remaud. Conditions to obtain precise and true measurements of the intramolecular  $^{13}\text{C}$  distribution  
1397 in organic molecules by isotopic  $^{13}\text{C}$  nuclear magnetic resonance spectrometry. Anal. Chim. Acta 846  
1398 (2014) 1–7. <https://doi.org/10.1016/j.aca.2014.07.018>
- 1399 65- B. Fry, J. F. Carter, K. Yamada, N. Yoshida, D. Juchelka. Position-specific  $^{13}\text{C}/^{12}\text{C}$  analysis of amino  
1400 acid carboxyl groups – automated flow-injection analysis based on reaction with ninhydrin. Rapid  
1401 Commun. Mass Spectrom. 32 (2018) 992–1000. <https://doi.org/10.1002/rcm.8126>
- 1402 66- A. P. Crawley, R. M. Henkemman. A comparison of one-shot and recovery methods in T1 imaging.  
1403 Magn. Reson. Med. 7 (1988) 23-34. <https://doi.org/10.1002/mrm.1910070104>.
- 1404 67- C. Liu, G. P. McGovern, P. Liua, H. Zhao, J. Horita. Position-specific carbon and hydrogen isotopic  
1405 compositions of propane from natural gases with quantitative NMR. Chem. Geol. 491 (2018) 14-26.  
1406 <https://doi.org/10.1016/j.chemgeo.2018.05.011>
- 1407 68- T. Wieloch, I. Ehlers, J. Yu, D. Franck, M. Grabner, A. Gessler, J. Schleucher. Intramolecular  $^{13}\text{C}$   
1408 analysis of tree rings provides multiple plant ecophysiology signals covering decades. Sci. Rep. 8  
1409 (2018) 5048 (10 pages). <https://doi.org/10.1038/s41598-018-23422-2>
- 1410 69- D. Hoffman, C. Rasmussen. Position-Specific carbon stable isotope ratios by proton NMR  
1411 spectroscopy. Anal. Chem. 91 (2019) 15661-15669. Doi: 10.1021/acs.analchem.9b03776
- 1412 70- E. P. Botosoa, E. Caytan, V. Silvestre, R. J. Robins, S. Akoka, G. S. Remaud. Unexpected  
1413 Fractionation in Site-Specific  $^{13}\text{C}$  Isotopic Distribution Detected by Quantitative  $^{13}\text{C}$  NMR at Natural  
1414 Abundance. J. Am. Chem. Soc. 130 (2008) 414-415. <https://doi.org/10.1021/ja0771181>
- 1415 71- M. Julien, J. Parinet, P. Nun, K. Bayle, P. Höhener, R. J. Robins, G. S. Remaud. Fractionation in  
1416 position-specific isotope composition during vaporization of environmental pollutants measured with  
1417 isotope ratio monitoring by  $^{13}\text{C}$  nuclear magnetic resonance spectrometry. Environ. Pollut. 205 (2015)  
1418 299-306. <http://dx.doi.org/10.1016/j.envpol.2015.05.047>

- 1419 72- M. Julien, P. Höhener, R. J. Robins, J. Parinet, G. S. Remaud. Position-Specific <sup>13</sup>C Fractionation  
1420 during Liquid–Vapor Transition Correlated to the Strength of Intermolecular Interaction in the Liquid  
1421 Phase. *J. Phys. Chem. B* 121 (2017) 5810–5817. DOI: 10.1021/acs.jpcc.7b00971
- 1422 73- E. P. Botosoa, V. Silvestre, R. J. Robins, J. M. Moreno Rojas, C. Guillou, G. S. Remaud. Evidence of  
1423 <sup>13</sup>C non-covalent isotope effects obtained by quantitative <sup>13</sup>C nuclear magnetic resonance  
1424 spectroscopy at natural abundance during normal phase liquid chromatography. *J. Chromatogr. A*  
1425 1216 (2009) 7043–7048. doi:10.1016/j.chroma.2009.08.066
- 1426 74- E. Cicchetti, V. Silvestre, W. Fieber, H. Sommer, G. Remaud, S. Akoka, A. Chaintreau. Procedure  
1427 for the isolation of vanillin from vanilla extracts prior to isotopic authentication by quantitative <sup>13</sup>C-  
1428 NMR. *Flavour Fragr. J.* 25 (2010) 463–467. DOI 10.1002/ffj.2006
- 1429 75- E. P. Botosoa, C. Blumenstein, D. A. MacKenzie, V. Silvestre, G. S. Remaud, R. A. Kwiecień, R. J.  
1430 Robins. Quantitative isotopic <sup>13</sup>C nuclear magnetic resonance at natural abundance to probe enzyme  
1431 reaction mechanisms via site-specific isotope fractionation: The case of the chain-shortening reaction  
1432 for the bioconversion of ferulic acid to vanillin. *Anal. Biochem.* 393 (2009) 182–188. doi:10.1016/  
1433 j.ab.2009.06.031
- 1434 76- A. Gilbert, R. J. Robins, G. S. Remaud, G. B. Tcherkez. Intramolecular <sup>13</sup>C pattern in hexoses from  
1435 autotrophic and heterotrophic C3 plant tissues. *Proc. Natl. Acad. Sci. U. S. A.* 109 (2012) 18204–  
1436 18209. <https://doi.org/10.1073/pnas.1211149109>
- 1437 77- D. G. Diomande, E. Martineau, A. Gilbert, P. Nun, A. Murata, K. Yamada, N. Watanabe, I. Tea, R. J.  
1438 Robins, N. Yoshida, G. S. Remaud. Position-Specific Isotope Analysis of Xanthines: A <sup>13</sup>C Nuclear  
1439 Magnetic Resonance Method to Determine the <sup>13</sup>C Intramolecular Composition at Natural  
1440 Abundance. *Anal. Chem.* 87 (2015) 6600–6606. DOI: 10.1021/acs.analchem.5b00559
- 1441 78- WHO 2017, <http://www.who.int/medicines/regulation/ssffc/definitions/en/>, consulted 1st April  
1442 2020
- 1443 79- K. Dégardin, Y. Roggo, P. Margot. Forensic intelligence for medicine anti-counterfeiting. *Forensic*  
1444 *Sci. Int.* 248 (2015) 15-17. <https://doi.org/10.1016/j.forsciint.2014.11.015>
- 1445 80- J. P. Jasper, B. J. Westenberger, J. A. Spencer, L. F. Buhse, M. Nasr. Stable isotopic  
1446 characterization of active pharmaceutical ingredients. *J. Pharm. Biomed. Anal.* 35 (2004) 21-29.  
1447 [https://doi.org/10.1016/S0731-7085\(03\)00581-8](https://doi.org/10.1016/S0731-7085(03)00581-8)
- 1448 81- T. Gilveska, M. Gehre, H. H. Richnow. Multidimensional isotope analysis of carbon, hydrogen and  
1449 oxygen as tool for identification of the origin of ibuprofen. *J. Pharm. Biomed. Anal.* 115 (2015) 410–  
1450 416. <https://doi.org/10.1016/j.jpba.2015.07.030>
- 1451 82- J. Gooch, B. Daniel, V. Abbate, N. Frascione. Taggant materials in forensic science: A review. *TrAC*  
1452 *Trends Anal. Chem.* 83 (2016) 49-5. <https://doi.org/10.1016/j.trac.2016.08.003>
- 1453 83- V. Silvestre, V. Maroga Mboula, C. Jouitteau, S. Akoka, R. J. Robins, G. S. Remaud. Isotopic <sup>13</sup>C  
1454 NMR spectrometry to assess counterfeiting of active pharmaceutical ingredients: Site-specific <sup>13</sup>C  
1455 content of aspirin and paracetamol. *J. Pharm. Biomed. Anal.* 50 (2009) 336-341. <https://doi.org/10.1016/j.jpba.2009.04.030>
- 1457 84- G. S. Remaud, U. Bussy, M. Lees, F. Thomas, J.-R. Desmurs, E. Jamin, V. Silvestre, S. Akoka. NMR  
1458 spectrometry isotopic fingerprinting: A tool for the manufacturer for tracking Active Pharmaceutical  
1459 Ingredients from starting materials to final medicines. *Eur. J. Pharm. Sci.* 48 (2013) 464–473.  
1460 <http://dx.doi.org/10.1016/j.ejps.2012.12.009>

1461 85- D. Acetti, E. Brenna, G. Fronza, C. Fuganti. Monitoring the synthetic procedures of commercial  
1462 drugs by  $^2\text{H}$  NMR spectroscopy: the case of ibuprofen and naproxen. *Talanta* 76 (2008) 651–655.  
1463 <https://doi.org/10.1016/j.talanta.2008.04.009>

1464 86- N. Gentile, R. T. W. Siegwolf, P. Esseiva, S. Doyle, K. Zollinger, O. Delémont. Isotope ratio mass  
1465 spectrometry as a tool for source inference in forensic science: A critical review. *Forensic Sci.*  
1466 *Internat.* 251 (2015) 139–158. <https://doi.org/10.1016/j.forsciint.2015.03.031>

1467 87- M. Julien, P. Nun, P. Höhener, J. Parinet, R. J. Robins, G. S. Remaud. Enhanced forensic  
1468 discrimination of pollutants by position-specific isotope analysis using isotope ratio monitoring by  $^{13}\text{C}$   
1469 nuclear magnetic resonance spectrometry. *Talanta* 147 (2016) 383–389. <https://doi.org/10.1016/j.talanta.2015.10.010>

1471 88- V. Joubert, V. Silvestre, V. Ladroue, F. Besacier, P. Blondel, S. Akoka, E. Baguet, G. S. Remaud.  
1472 Forensic application of position-specific isotopic analysis of trinitrotoluene (TNT) by NMR to  
1473 determine  $^{13}\text{C}$  and  $^{15}\text{N}$  intramolecular isotopic profiles. *Talanta*, 2020, in press. [https://doi.org/](https://doi.org/10.1016/j.talanta.2020.120819)  
1474 [10.1016/j.talanta.2020.120819](https://doi.org/10.1016/j.talanta.2020.120819)

1475 89- V. Joubert, M. Trébuchet, M. Mikic, V. Silvestre, A.-M. Schiphorst, D. Loquet, A. Stemmel, V.  
1476 Ladroue, F. Besacier, S. Akoka, G. S. Remaud. Isotopomics by isotope ratio monitoring by  $^{13}\text{C}$  nuclear  
1477 magnetic resonance spectrometry on cutting agents in heroin: A new approach for illicit drugs  
1478 trafficking route elucidation. *Drug Test. Anal.*, 2020, in press. <https://doi.org/10.1002/dta.2745>

1479 90- M. M. Bomgardner. The problem with vanilla. *Chem. Eng. News* 94 (2016) 38–42.

1480 91- J. Bricout, J. Koziat, M. Derbesy, B. Becat. Nouvelles possibilités de l'analyse des isotopes stables  
1481 du carbone dans le contrôle de la qualité des vanilles. *Ann. Fals. Exp. Chim.* 74 (1981) 691–696.

1482 92- G. S. Remaud, Y.-L. Martin, G. G. Martin, G. J. Martin. Detection of Sophisticated Adulterations of  
1483 Natural Vanilla Flavors and Extracts: Application of the SNIF-NMR Method to Vanillin and p-  
1484 Hydroxybenzaldehyde. *J. Agric. Food Chem.* 45 (1997) 859–866. <https://doi.org/10.1021/jf960518f>

1485 93- E. Jamin, F. Martin, G. G. Martin, A.-I. Fauhl. Determination of Site-Specific (Deuterium/  
1486 Hydrogen) Ratios in Vanillin by  $^2\text{H}$ -Nuclear Magnetic Resonance Spectrometry: Collaborative Study. *J.*  
1487 *AOAC Int.* 90 (2007) 187–195. <https://doi.org/10.1093/jaoac/90.1.187>

1488 94- N. J. Gallage, B. L. Møller. Vanillin—bioconversion and bioengineering of the most popular plant  
1489 flavor and its de novo biosynthesis in the vanilla orchid. *Molecular Plant.* 8 (2015) 40–57.  
1490 <https://doi.org/10.1016/j.molp.2014.11.008>

1491 95- G. Hajjar, T. Rizk, J. Bejjani, S. Akoka. Metabisotopomics of triacylglycerols from animal origin: A  
1492 simultaneous metabolomic and isotopic profiling using  $^{13}\text{C}$  INEPT. *Food Chem.* 315 (2020) 126325.  
1493 <https://doi.org/10.1016/j.foodchem.2020.126325>

1494 96- N. Merchak, T. Rizk, V. Silvestre, G. S. Remaud, J. Bejjani, S. Akoka. Olive oil characterization and  
1495 classification by  $^{13}\text{C}$ -NMR with a polarization transfer technique: A comparison with gas  
1496 chromatography and  $^1\text{H}$ -NMR. *Food Chem.* 245 (2018) 717–723. [https://doi.org/10.1016/](https://doi.org/10.1016/j.foodchem.2017.12.005)  
1497 [j.foodchem.2017.12.005](https://doi.org/10.1016/j.foodchem.2017.12.005)

1498 97- M. H. Thiemens. Introduction to Chemistry and Applications in Nature of Mass Independent  
1499 Isotope Effects Special Feature. *Proc. Natl. Acad. Sci. U. S. A.* 110 (2013) 17631–17637.  
1500 [https://doi.org/ 10.1073/pnas.1312926110](https://doi.org/10.1073/pnas.1312926110)

1501

***Acronyms and symbols for NMR***

$\beta$	Flip angle
$\vec{B}_0$	Static magnetic field
$\vec{B}_1$	RF magnetic field
$\vec{B}_2$	RF magnetic field during decoupling
$\gamma$	Magnetogyric ratio
DEPT	Distortionless enhancement by polarization transfer
DMSO-d <sub>6</sub>	Dimethylsulfoxide fully deuterated
FS-INEPT	Full spectrum insensitive nuclei enhancement by polarization transfer
$\Gamma$	Difference from 1 in the ratio of CH <sub>2</sub> /CH <sub>3</sub> in <sup>13</sup> C bi-labeled ethanol
HSQC	Heteronuclear single quantum coherence
<i>i</i>	Position of the atom within the molecule (found also as site)
INEPT	Insensitive nuclei enhancement by polarization transfer
<i>M</i>	Magnetization
<i>M<sub>eq</sub></i>	Magnetization at equilibrium (steady state)
nD	NMR at dimension n
<i>n<sub>i</sub></i>	Equivalent number of nuclei at position i
NMR	Nuclear magnetic resonance
nOe	Nuclear Overhauser effect
OIA	Offset-independent-adiabaticity
$\Omega$	Signal offset
qNMR	Quantitative Nuclear magnetic resonance
RF	Radio-frequency
S	Area of NMR peak



SNR	Signal-to-noise ratio
$T_a$	Analysis time
$T_1$	Longitudinal relaxation time
$T_2$	Transverse relaxation time
$TI$	Inversion time
$TR$	Repetition time: delay between consecutive acquisition in the pulse sequence
$\omega_1$	Amplitude ( $\gamma \cdot B_1$ ) in Hertz of RF pulses
$\omega_2$	Amplitude ( $\gamma \cdot B_2$ ) in Hertz of RF pulses during heteronuclear decoupling
WALTZ	Wideband alternating-phase low-power technique for zero residual splitting

### ***Acronyms and symbols for isotopic composition***

IRMS	Isotope ratio mass spectrometry
irm-NMR	Isotope ratio measured by Nuclear magnetic resonance
irm-MS	Isotope ratio measured by Mass spectrometry
LC-irm-MS	Liquid chromatography coupled to isotope ratio measured by Mass spectrometry
GC-irm-MS	Gas chromatography coupled to isotope ratio measured by Mass spectrometry
CSIA	Compound-specific isotope analysis
PSIA	Position-specific isotope analysis
SNIF-NMR	Site-specific natural isotopic fractionation measured by Nuclear magnetic resonance
$f_i$	Experimental isotopomer molar fraction as the ratio of the area of peak $i$ to the total area of all peaks in the molecule determined by NMR
$F_i$	Statistical molecular fraction as the molar fraction for the carbon position $i$ , in case of a homogeneous $^{13}\text{C}$ distribution within the molecule
$\delta$	Isotopic composition (not to be confused with the chemical shift)
$\delta_g$	Global isotopic composition as obtained by IRMS
$\delta_i$	Isotopic composition at position $i$

$^hE$	Heavier isotopes of the element $E$
$^lE$	Lighter isotopes of the element $E$
$R$	Isotopic ratio
$x$	Isotopic abundance
$E$	Element
V-PDB	Vienna-Pee dee Belemnite
KIE	Kinetic isotope effect
EIE	Equilibrium isotope effect
$\alpha$	Isotope effect
$\Delta$	Isotopic fractionation
$\varepsilon$	Isotope enrichment
‰	Per mil, <i>e.g.</i> 1‰ = 0.1%

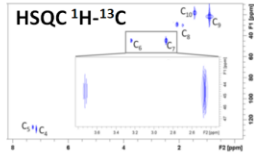
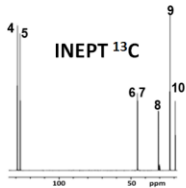
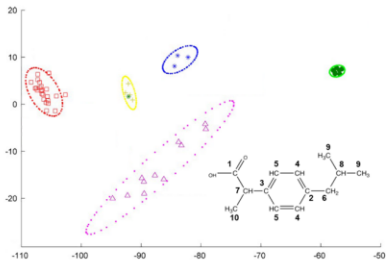
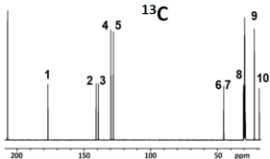
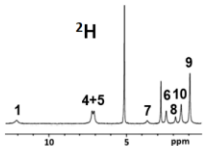
### ***Other acronyms and symbols***

API	Active pharmaceutical ingredient
C	Molar concentration
C <sub>3</sub>	One of the three metabolic pathways for carbon fixation in photosynthesis
C <sub>4</sub>	One of the three metabolic pathways for carbon fixation in photosynthesis
CAM	One of the three metabolic pathways for carbon fixation in photosynthesis (Crassulacean Acid Metabolism)
ETBE	Ethyl <i>tert</i> -butyl ether
E	Error due to partial saturation
IAEA	International Atomic Energy Agency
$m$	Weight, in NMR tube preparation
$M$	Molar mass
MDMA	3,4-methylenedioxy-N-methylamphetamine, commonly known as ecstasy

MTBE	Methyl <i>tert</i> -butyl ether
PCA	Principal component analysis
sn1	Substitution at position 1 of glycerol
sn2	Substitution at position 2 of glycerol
sn3	Substitution at position 3 of glycerol
TAME	<i>tert</i> -amyl methyl ether
TCE	Trichloroethene
TNT	Trinitrotoluene
VIM	International vocabulary of metrology
WHO	World Health Organization
ξ	Required accuracy
sinc	$\frac{\sin(a)}{a}$

1503

# NMR based isotopomics



# 2020 年 1 月 1 日

